

NACA RM 3450A05

FOR REFERENCE

NOT TO BE TAKEN FROM THIS ROOM

NACA

RESEARCH MEMORANDUM

for the

Air Materiel Command, U. S. Air Force

TESTS OF THE NORTHROP XSSM-A-3 MISSILE IN

THE AMES 40- BY 80-FOOT WIND TUNNEL. -

WING MODIFICATIONS

By David Graham

Ames Aeronautical Laboratory  
Moffett Field, Calif.

CLASSIFICATION CHANGED

UNCLASSIFIED

To

100A Report RN-125

signature Feb 26/1958  
CLASSIFIED DOCUMENT

By authority of

AMT 3-24-58

This report contains classified information...  
The National Aeronautics and Space Administration...  
is authorized to disseminate this information...  
to persons in the military and naval...  
service of the United States, and to...  
civilian officials and members of the Federal...  
Bureau of Investigation, and to...  
State officials of friendly...  
countries and their...  
citizens.

NATIONAL ADVISORY COMMITTEE  
FOR AERONAUTICS

WASHINGTON

Jan. 5, 1950

52117  
711-11-11  
- 5311-11-11

CLASSIFIED DOCUMENT  
UNCLASSIFIED  
100A Report RN-125  
AMT 3-24-58

8/198



## NATIONAL ADVISORY COMMITTEE FOR AERONAUTICS

RESEARCH MEMORANDUM

for the

Air Materiel Command, U S Air Force

TESTS OF THE NORTHROP XSSM-A-3 MISSILE IN THE

AMES 40- BY 80-FOOT WIND TUNNEL.--

WING MODIFICATIONS

By David Graham

## SUMMARY

Wind-tunnel tests were conducted to determine the longitudinal stability characteristics of a full-scale Northrop XSSM-A-3 missile. Various wing modifications were investigated in an effort to provide a configuration that would maintain longitudinal stability to lift coefficients necessary for landing the missile during flight tests. The results of the tests led to the choice of a wing with an increased leading-edge radius. A short discussion of the results is presented, but no analysis of the data has been made in order to make the data available as soon as possible.

## INTRODUCTION

Small-scale tests of the Northrop XSSM-A-3, a long-range missile designed to fly at high subsonic speeds, have shown it to be longitudinally unstable at lift coefficients above 0.45 due to tip stall of the swept-back wings. A number of missiles have been built for use in free-flight tests and are to be recovered by landing. The landing requirements are that the missile be stable to lift coefficients above 0.6 and that the ground angle be less than  $0^\circ$ , neither of which are met by the basic configuration as indicated by the small-scale tests.

Therefore, at the request of the Air Materiel Command, U.S. Air Force, an investigation of the full-scale XSSM-A-3 was made in the Ames 40- by 80-foot wind tunnel. The tests were to determine whether the aeroelasticity and Reynolds numbers of the full-scale wing would



alleviate the tip stall and thus maintain stability to the desired lift coefficients, or whether it would be necessary to modify the wing to obtain the desired results.

### NOTATION

The results of the tests are presented as standard NACA coefficients of forces and moments. The coefficients and symbols are defined below and in figure 1:

- A aspect ratio  $\left(\frac{b^2}{S}\right)$
- b wing span, feet
- c wing chord, measured perpendicular to the 40-percent-chord line, feet
- $c_s$  wing chord, measured parallel to the plane of symmetry of the missile, feet
- $\bar{c}_s$  mean aerodynamic chord, measured parallel to the plane of symmetry of the missile  $\left(\frac{\int_0^{b/2} c_s^2 dy}{\int_0^{b/2} c_s dy}\right)$ , feet
- $C_L$  lift coefficient  $\left(\frac{\text{lift}}{qS}\right)$
- $C_D$  drag coefficient  $\left(\frac{\text{drag}}{qS}\right)$
- $C_{DT}$  increment of drag due to wind-tunnel-wall interference
- $C_m$  pitching-moment coefficient  $\left(\frac{\text{pitching moment}}{qS\bar{c}_s}\right)$
- q free-stream dynamic pressure, pounds per square foot
- R Reynolds number  $\left(\frac{V\bar{c}_s}{\nu}\right)$
- S wing area, square feet
- V free-stream velocity, feet per second
- y spanwise distance outboard from wing center line, feet (unless otherwise noted)

- $\alpha$  free-stream angle of attack, with reference to the wing-chord plane, degrees
- $\alpha_T$  increment of angle of attack due to wind-tunnel-wall interference, degrees
- $\delta_f$  trailing-edge split-flap deflection, measured perpendicular to the hinge line, degrees
- $\nu$  kinematic viscosity, square feet per second

#### DESCRIPTION OF MISSILE AND APPARATUS

The investigation of the Northrop XSSM-A-3 missile was conducted in the Ames 40- by 80-foot wind tunnel. A three-view drawing of the missile is shown in figure 2 and additional dimensional data are given in table I. The airfoil sections perpendicular to the 40-percent-chord line were modified NACA 65-009 sections. The modification consisted of fairing the section from the 66-percent-chord point to the trailing edge by straight lines. Ordinates of the section are given in table II.

The wing was modified in a number of ways. The modifications consisted of (1) single fences mounted on each wing; (2) double fences mounted on each wing; (3) 30-percent, 60-percent, and full-span leading-edge flaps with the partial-span flaps being mounted on the outboard portion of the wing; and (4) an increased leading-edge radius. Details of these wing modifications are shown in figures 3, 4, 5, and 6, respectively. The purpose of the leading-edge flap was to simulate, for the subject tests, the effects of nose camber that would be obtained by use of an NACA 430 mean camber line. For the sake of simplicity, only the forward portion of the upper surface of the resultant airfoil section was formed and was shifted forward and down until its upper surface and effective camber line were tangent to those of the existing airfoil. The wing was also equipped with inboard trailing-edge split flaps and outboard elevons which are shown in figure 2. Photos of the model mounted in the tunnel and of some of the various configurations, or combinations thereof, that were tested are shown in figure 7. The fuselage had an NACA submerged-type inlet on the bottom surface which was faired over for the tests. Small deflectors around the inlet were left on for the tests (fig. 7(g)). The tail-pipe exit was covered by a fairing upon which was mounted a camera box which was to be used in later tests (figs. 2 and 7(c)).

#### TESTS AND RESULTS

The tests conducted and the configurations tested are listed in table III which also serves as an index to figures 8 to 17 in which

the data are presented. Tests were made at dynamic pressures of 5, 25, 48, and 72 pounds per square foot, which resulted in Reynolds numbers of approximately 3.0, 6.6, 9.0, and  $11.0 \times 10^6$ , respectively, as based on the mean aerodynamic chord.

The dimensions of the missile as listed in table I were used in reducing the data to coefficient form. The pitching-moment coefficients are referred to a moment center located 1 inch above the longitudinal fuselage axis, and 256.81 inches aft of the fuselage nose. The fore and aft location corresponds to the longitudinal station of the quarter-chord of the mean aerodynamic chord.

The angles of attack and the drag coefficients have been corrected for stream-angle inclination and for wind-tunnel-wall effect, the latter correction being that for a wing of the same span having elliptic loading but with an unswept plan form. The following corrections were applied:

$$\alpha_T = 0.598 C_L$$

$$C_{DT} = 0.0104 C_L^2$$

No drag or pitching-moment tares were applied to the data, since the drag of the support fittings in the presence of the wing and the interference effects between the fuselage and the fittings are unknown. The drag tare of the exposed part of the support-strut tips including the ball sockets is of the order 0.0046 based on the missile wing dimensions. This drag tare was obtained without a model in the tunnel. In addition, the camera cover, which was mounted on the fuselage tail fairings aft of the vertical tail, gave an increment of drag of 0.0028 at zero angle of attack.

A feature of the test results to which attention should be called is the erratic variations of pitching-moment coefficient. The test points shown in the figures are the average of five separate balance readings which were obtained at approximately 5-second intervals. A check of a number of the pitching-moment-coefficient test points showed a variation of as much as 0.01 in the coefficient for the five balance readings taken. This variation may be a result of a slight yawing oscillation of the missile due to the required close spacing of the support struts and the resultant unsteadiness of the support system. Despite this variation, the lift coefficients at which the breaks in the pitching-moment curves occurred are well defined.

Throughout the tests reported herein, the elevons were to be maintained in the undeflected position. An attempt was made to hold the elevons by means of remotely controlled servo units. This method was effective for the first tests (fig. 8), but during the tests with the single fence configuration (fig. 9) the undeflected elevon positions could not be maintained, resulting in the shifts of the pitching-moment curves. The actual type of variation, whether sudden or gradual,

is not known. For the remainder of the tests, the elevons were clamped in the undeflected position.

#### DISCUSSION

The landing requirements for the missile were that the missile should be longitudinally stable up to a lift coefficient of at least 0.6 and that the ground angle at this lift coefficient be  $9^\circ$  or less. The results of the tests of the basic full-scale missile (fig. 8) indicate, in agreement with small-scale tests, that neither condition was satisfied. Longitudinal instability is evident below a lift coefficient of 0.6 for all four sets of test conditions, indicating that the aeroelastic and/or Reynolds number effects of the full-scale wing did not alleviate the tip stall. In addition, the ground angle is in excess of  $9^\circ$  (assuming that the ground angle is equal to the angle of attack). Therefore, a number of modifications including single fences, double fences, leading-edge flaps, and increased leading-edge radius were tested. The results of these tests are shown in figures 9 to 15. Comparisons of the effects of these various devices at a Reynolds number of approximately  $9 \times 10^6$  are shown in figure 16. These results show that neither fence configuration was effective in extending the stable portion of the pitching-moment curves above a lift coefficient of 0.6; whereas the increased leading-edge radius and the full-span leading-edge flaps were effective to approximately 0.8 and 0.9, respectively. The angle of attack for a lift coefficient of 0.6 was, however, still in excess of the allowable  $9^\circ$ . The addition of trailing-edge flaps deflected  $15^\circ$  (fig. 16(b)) resulted in a satisfactory angle of attack, about  $8^\circ$ , and extended the stable portion of the pitching-moment curves to lift coefficients of 0.9 and 1.05 for the increased leading-edge radius and leading-edge flaps, respectively.

The final configuration chosen was that of the increased leading-edge radius with the trailing-edge flaps. The reason for the choice of the increased leading-edge radius over the leading-edge flaps was that, by merely increasing the leading-edge radius, satisfactory longitudinal stability characteristics could be obtained without paying a drag penalty at low lift coefficients. In addition, it was believed that, in the event it was desired to extend the flight tests to higher speeds, the increased nose radius would be more acceptable since there would be less likelihood that it would seriously affect the high-speed characteristics of the wing. The trailing-edge flaps are to be left undeflected for the flights and are to be deflected immediately prior to landing in order to decrease the angle of attack necessary to obtain a given lift coefficient. Comparisons of the characteristics of the basic configuration with those of the final configuration are shown in figure 17.

Ames Aeronautical Laboratory,  
National Advisory Committee for Aeronautics,  
Moffett Field, Calif.

TABLE I.— GEOMETRIC DATA OF THE MISSILE

Wing	
Span, feet . . . . .	42.26
Area, square feet . . . . .	300
Mean aerodynamic chord, feet . . . . .	7.51
Angle of incidence, degrees . . . . .	0
Aspect ratio . . . . .	6
Taper ratio . . . . .	0.4
Fuselage	
Length, feet . . . . .	52.67
Maximum diameter, feet . . . . .	4.83

TABLE II.— COORDINATES OF THE MODIFIED  
NACA 65-009 SECTION

Station (percent chord)	Ordinate (percent chord)
0	0
.50	.700
.75	.845
1.25	1.058
2.50	1.421
5.00	1.961
7.50	2.383
10.00	2.736
15.00	3.299
20.00	3.727
25.00	4.050
30.00	4.282
35.00	4.431
40.00	4.496
45.00	4.469
50.00	4.336
55.00	4.086
60.00	3.743
65.00	3.328
66.00 <sup>a</sup>	3.241
100.00	0

L.E. Radius: 0.552

<sup>a</sup>Section faired from 66-percent-chord point to the trailing edge by straight lines.

TABLE III.- SUMMARY OF CONFIGURATIONS TESTED

Figure	Configuration	Reynolds number
8	Basic missile	3.04 × 10 <sup>6</sup> 6.60 8.92 10.50
9	Single fences	3.06 × 10 <sup>6</sup> 6.45 9.40 11.13
10(a)	Double fences	3.04 × 10 <sup>6</sup> 6.83 8.84 10.78
10(b)	Double fences Double fences; $\delta_f$ , 15° Double fences; $\delta_f$ , 30° Double fences; $\delta_f$ , 45°	9 × 10 <sup>6</sup>
11	Full-span leading-edge flaps	2.99 × 10 <sup>6</sup> 6.68 9.18 11.44
12	Full-span leading-edge flaps Full-span leading-edge flaps; $\delta_f$ , 15° Full-span leading-edge flaps; $\delta_f$ , 15°; single fences	9 × 10 <sup>6</sup>
13(a)	Full-span leading-edge flaps 60-percent-span leading-edge flaps 30-percent-span leading-edge flaps	9 × 10 <sup>6</sup>
13(b)	Full-span leading-edge flaps; $\delta_f$ , 15° 60-percent-span leading-edge flaps; $\delta_f$ , 15° 30-percent-span leading-edge flaps; $\delta_f$ , 15°	9 × 10 <sup>6</sup>
14	Increased leading-edge radius	3.04 × 10 <sup>6</sup> 6.67 9.33 11.27

TABLE III.- CONCLUDED

Figure	Configuration	Reynolds number
15(a)	Increased leading-edge radius; double fences	6.78 × 10 <sup>6</sup> 9.39 11.23
15(b)	Increased leading-edge radius Increased leading-edge radius; double fences Increased leading-edge radius; δ <sub>f</sub> , 15° Increased leading-edge radius; double fences; δ <sub>f</sub> , 15°	9 × 10 <sup>6</sup>
16(a)	Basic missile Single fences Double fences Full-span leading-edge flaps Increased leading-edge radius	9 × 10 <sup>6</sup>
16(b)	Basic missile Double fences: δ <sub>f</sub> , 15° Full-span leading-edge flaps; δ <sub>f</sub> , 15° Increased leading-edge radius; δ <sub>f</sub> , 15°	9 × 10 <sup>6</sup>
17	Basic missile Increased leading-edge radius Increased leading-edge radius; δ <sub>f</sub> , 15°	9 × 10 <sup>6</sup>

[REDACTED]  
FIGURE LEGENDS

Figure 1.- Sign convention for the standard NACA coefficients. The forces, moment, angles, and control-surface deflection are shown as positive.

Figure 2.- Three-view drawing of the Northrop XSSM-A-3 Missile.

Figure 3.- Details of the single-fence configuration.

Figure 4.- Details of the double-fence configuration.

Figure 5.- Details of the leading-edge flap configuration.

Figure 6.- Details of the increased leading-edge radius configuration.

Figure 7.- Photographs of the configurations tested. (a) General view with single fences.

Figure 7.- Continued. (b) Close-up of single fences.

Figure 7.- Continued. (c) Close-up of double fences.

Figure 7.- Continued. (d) Close-up of lower surface of right wing with full-span leading-edge flap and trailing-edge flap deflected  $45^\circ$ .

Figure 7.- Continued. (e) Close-up of lower surface of right wing with 30-percent-span leading-edge flap.

Figure 7.- Continued. (f) Close-up of lower surface of right wing with increased leading-edge radius.

Figure 7.- Concluded. (g) General view of model with increased leading-edge radius.

Figure 8.- Aerodynamic characteristics of the basic model. Without trailing-edge flaps; various Reynolds numbers.

Figure 9.- Aerodynamic characteristics of the model with single fences. Without trailing-edge flaps; various Reynolds numbers.

Figure 10.- Aerodynamic characteristics of the model with double fences. (a) Without trailing-edge flaps; various Reynolds numbers.

Figure 10.- Concluded. (b) Trailing-edge flaps;  $R, 9 \times 10^6$ .

Figure 11.- Aerodynamic characteristics of the model with full-span leading-edge flaps; various Reynolds numbers.

[REDACTED]

Figure 12.-- Aerodynamic characteristics of the model with full-span leading-edge flaps in combination with trailing-edge flaps and single fences.  $R, 9 \times 10^6$ .

Figure 13.-- Aerodynamic characteristics of the model with various spans of leading-edge flaps.  $R, 9 \times 10^6$ . (a) Without trailing-edge flaps.

Figure 13.-- Concluded. (b) Trailing-edge flaps,  $15^\circ$ .

Figure 14.-- Aerodynamic characteristics of the model with increased leading-edge radius. Various Reynolds numbers.

Figure 15.-- Aerodynamic characteristics of the model with increased leading-edge radius. (a) Without trailing-edge flaps; various Reynolds numbers; double fences.

Figure 15.-- Concluded. (b) Various configurations;  $R, 9 \times 10^6$ .

Figure 16.-- Comparison of the aerodynamic characteristics of various configurations tested.  $R, 9 \times 10^6$ . (a) Without trailing-edge flaps.

Figure 16.-- Concluded. (b) Trailing-edge flaps,  $15^\circ$ .

Figure 17.-- Comparison of the aerodynamic characteristics of the basic model with the characteristics of the model with increased leading-edge radius, with and without trailing-edge flaps.  $R, 9 \times 10^6$ .

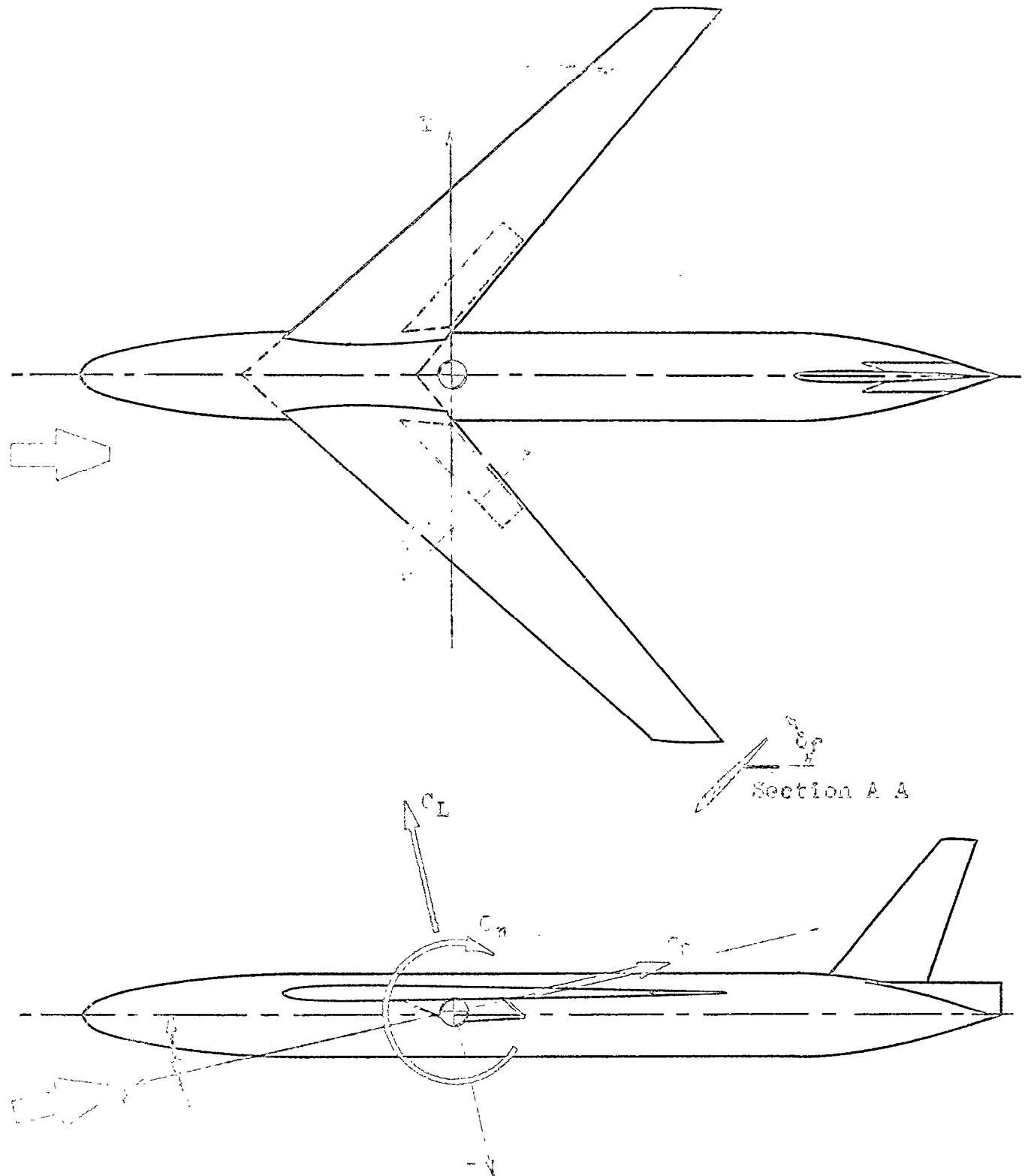


Figure 1 Diagram illustrating the forces and moments acting on a streamlined body in a flow field. The forces shown are lift ( $C_L$ ), drag ( $C_D$ ), side force ( $C_Y$ ), and normal force ( $C_N$ ). The moments shown are the pitching moment ( $M$ ) and the yawing moment ( $N$ ). The diagram also shows the chord line and the spanwise direction.

ALL DIMENSIONS IN INCHES UNLESS OTHERWISE NOTED

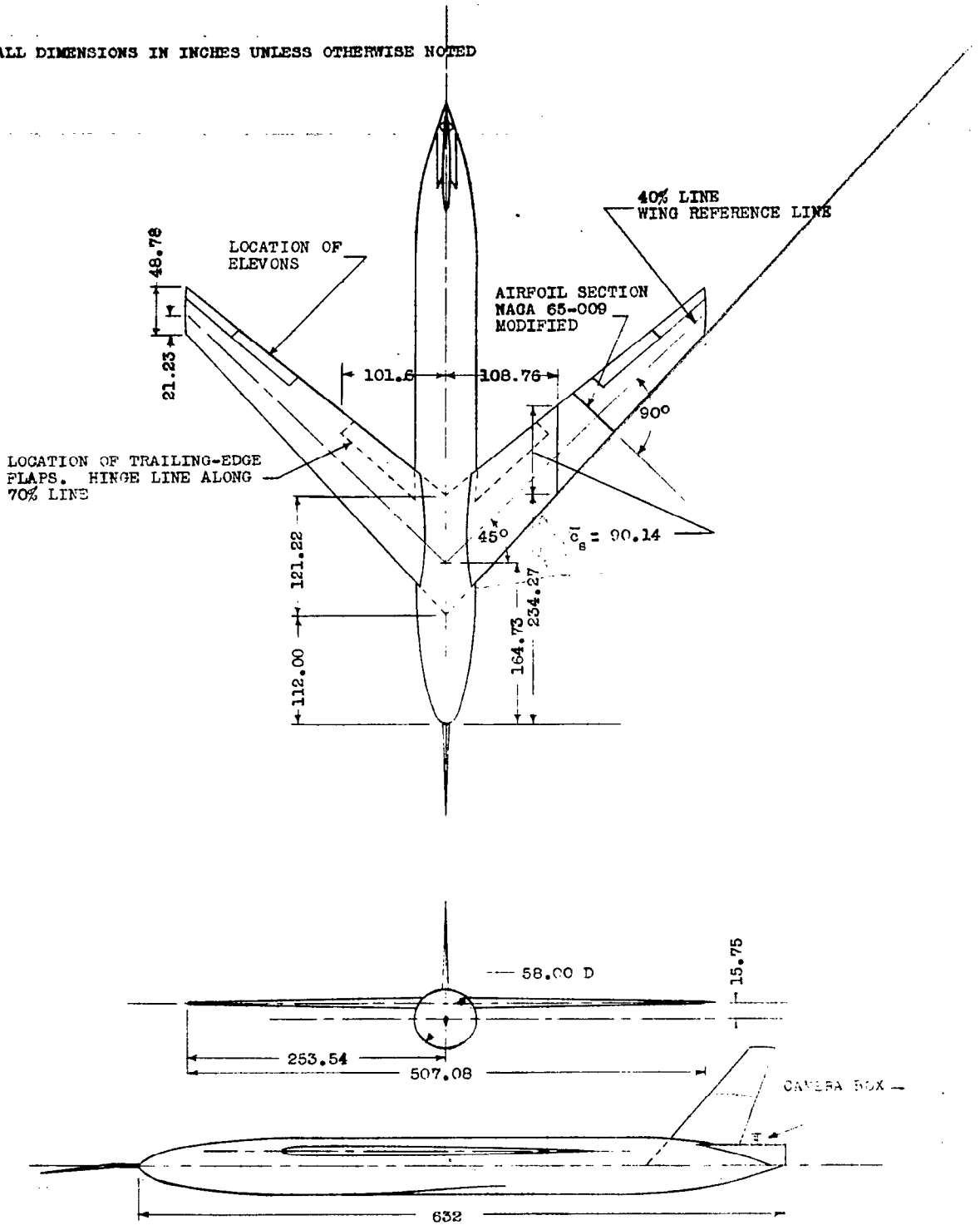
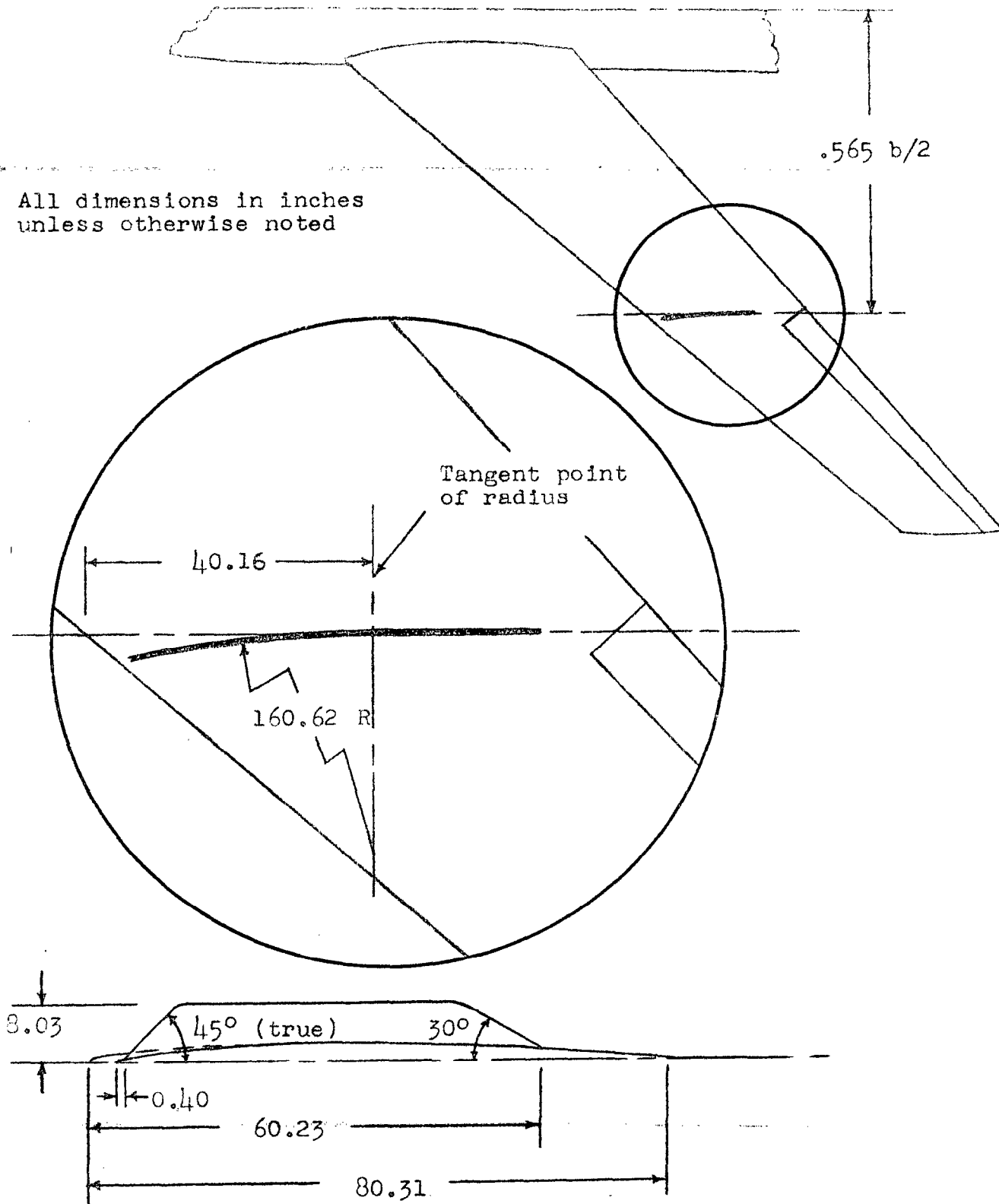
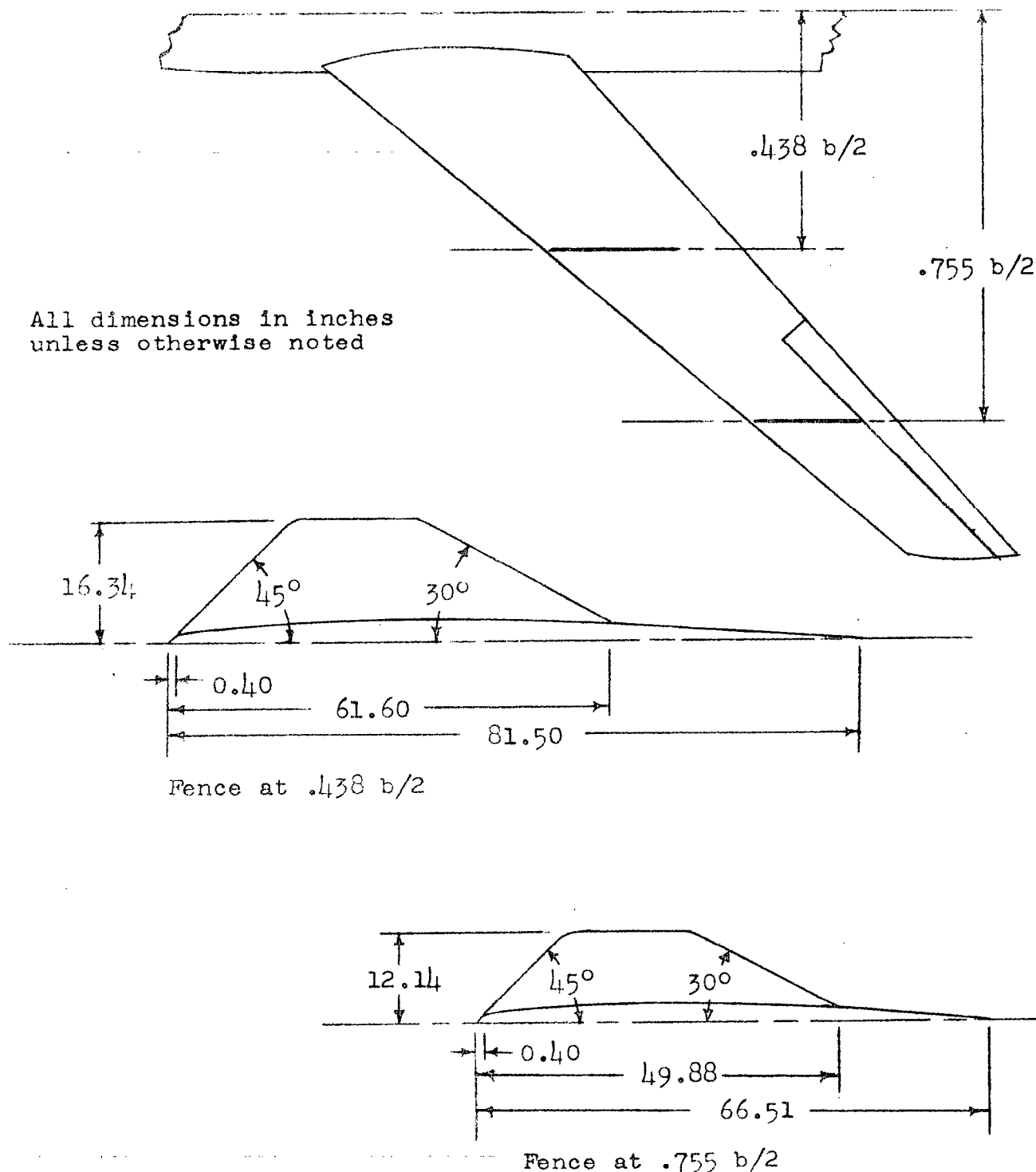


FIGURE 2.- THREE-VIEW DRAWING OF THE NORTHROP XSSM-A-3 MISSILE.

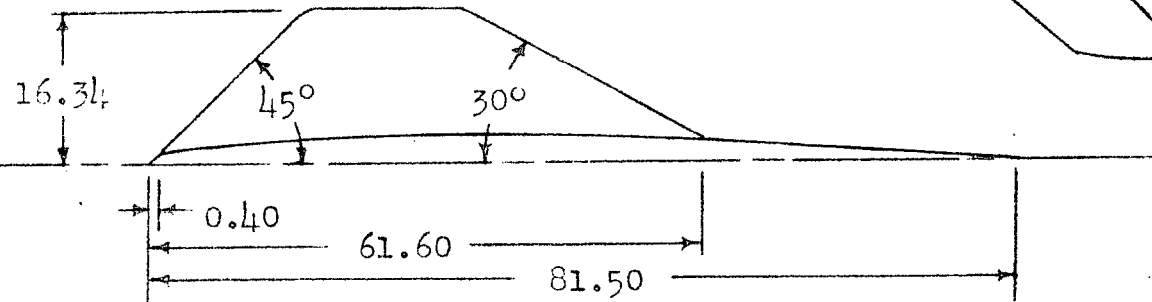


All dimensions in inches unless otherwise noted

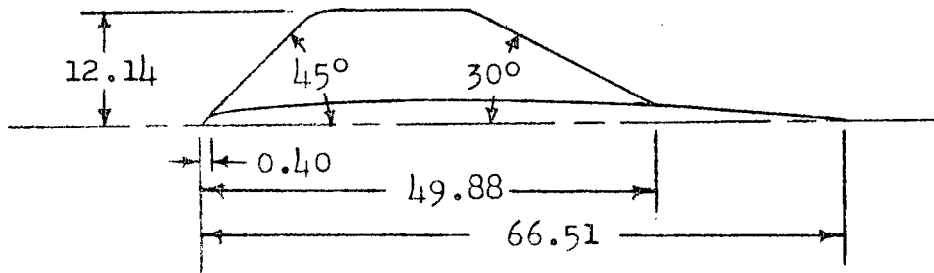
Figure 3.- Details of the single-fence configuration.



All dimensions in inches unless otherwise noted

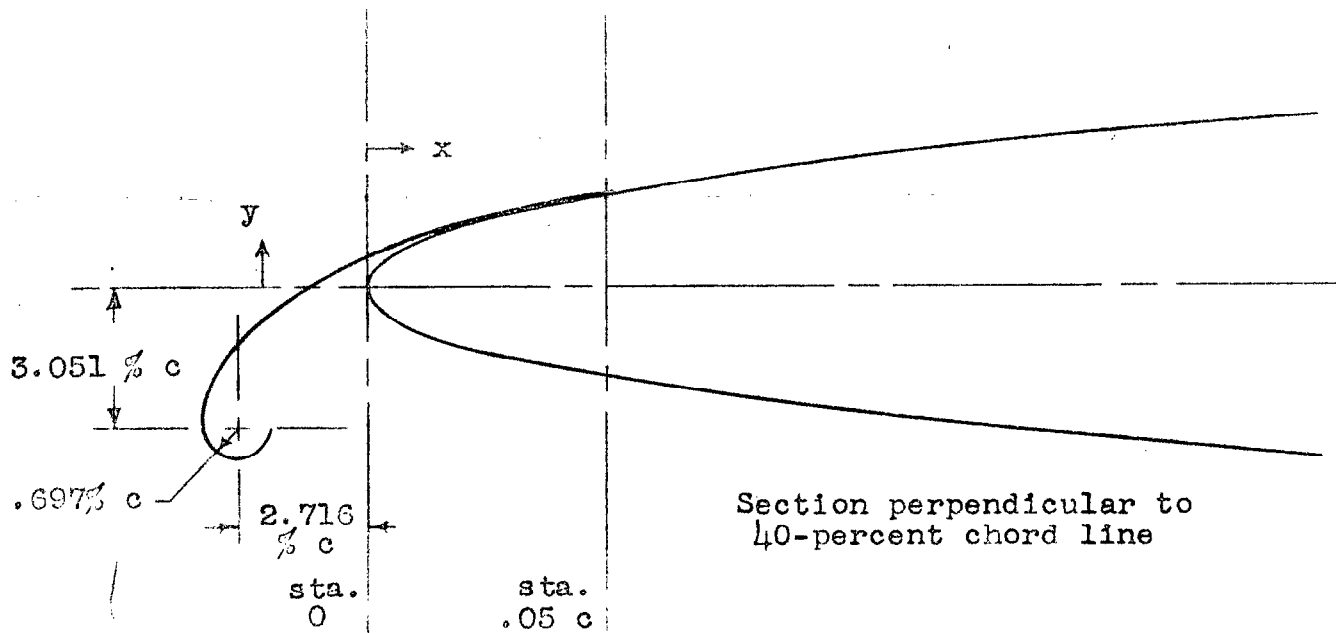


Fence at  $.438 b/2$



Fence at  $.755 b/2$

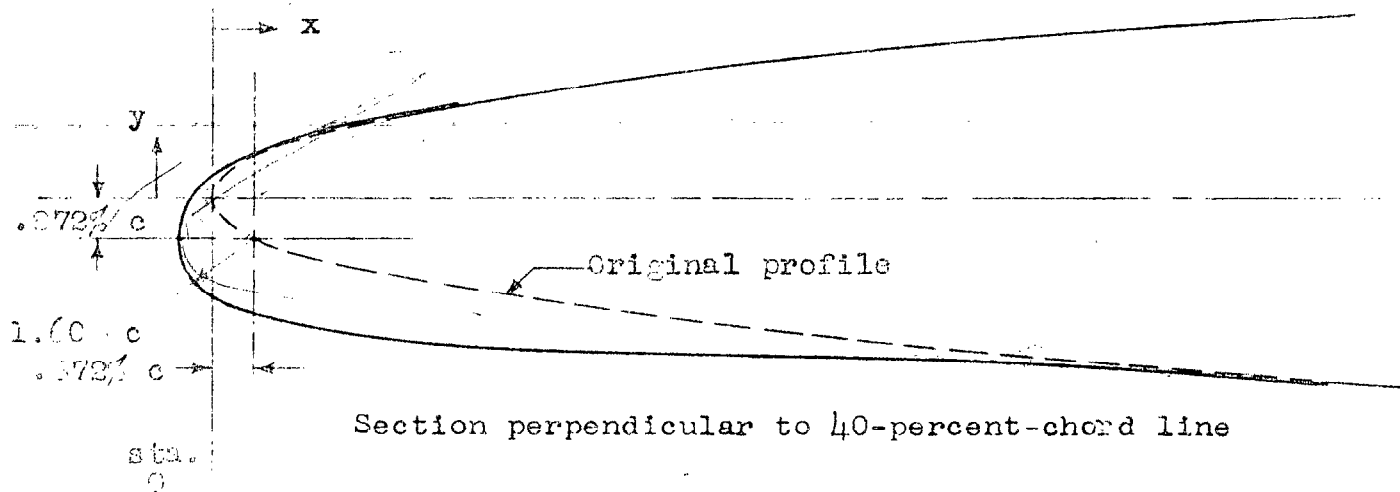
Figure 4. - Details of the double-fence configuration.



ORDINATES

x	y
Percent of Chord	Percent of Chord
-3.443	-2.833
-3.341	-2.339
-2.978	-1.584
-2.615	-1.118
-2.252	-.741
-1.888	-.435
-1.162	.065
-.435	.465
0	.669
.727	.959
1.453	1.221
2.180	1.424
2.906	1.600
3.633	1.743
4.358	1.874
5.085	1.998

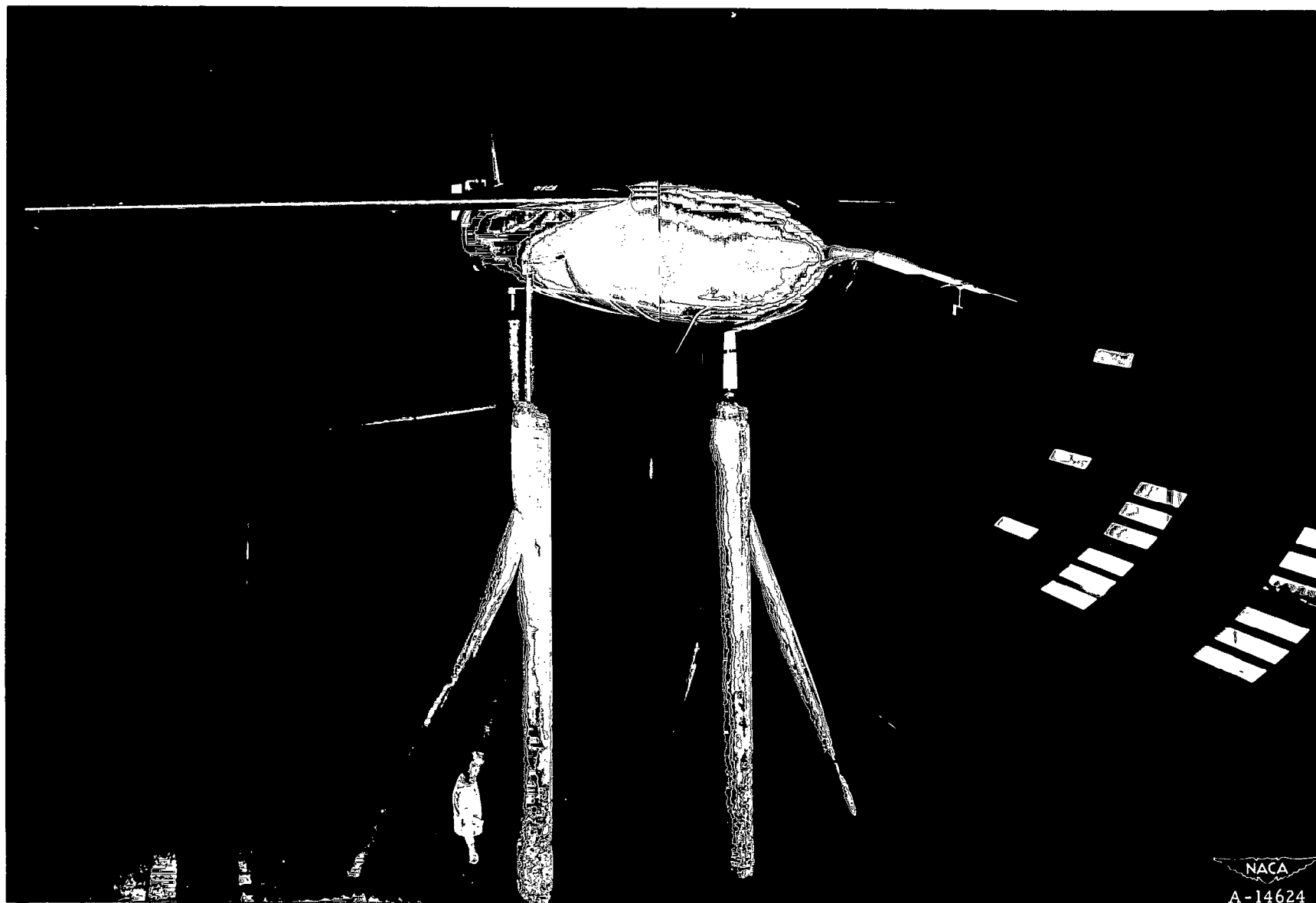
Figure 5.- Details of the leading-edge flap configuration.



COORDINATES

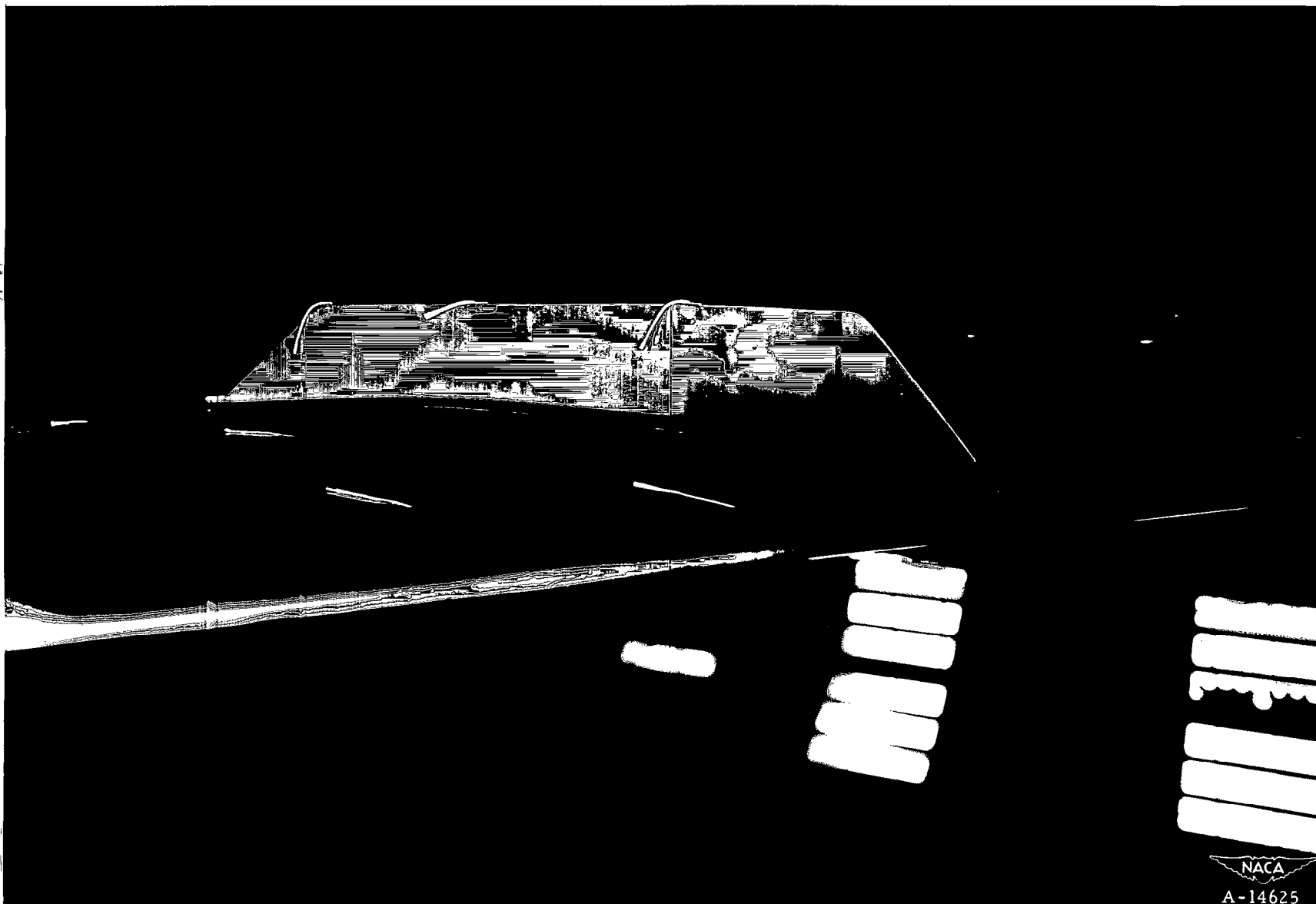
x	y <sub>upper</sub>	y <sub>lower</sub>
Percent of Chord	Percent of Chord	Percent of Chord
-0.727	-0.872	-0.872
-.363	.145	-1.816
0	.465	-2.136
.363	.697	-2.339
.727	.936	-2.477
1.453	1.191	-2.674
2.180	1.357	-2.826
3.633	1.729	-3.065
5.085	2.005	-3.219
6.538		-3.305
7.991		-3.385
10.171		-3.458
12.349		-3.508
14.529		-3.537
16.708		-3.596
18.888		-3.719
21.068		-3.865
23.246		-3.981

Figure C. - Details of the increased leading-edge radius configuration.



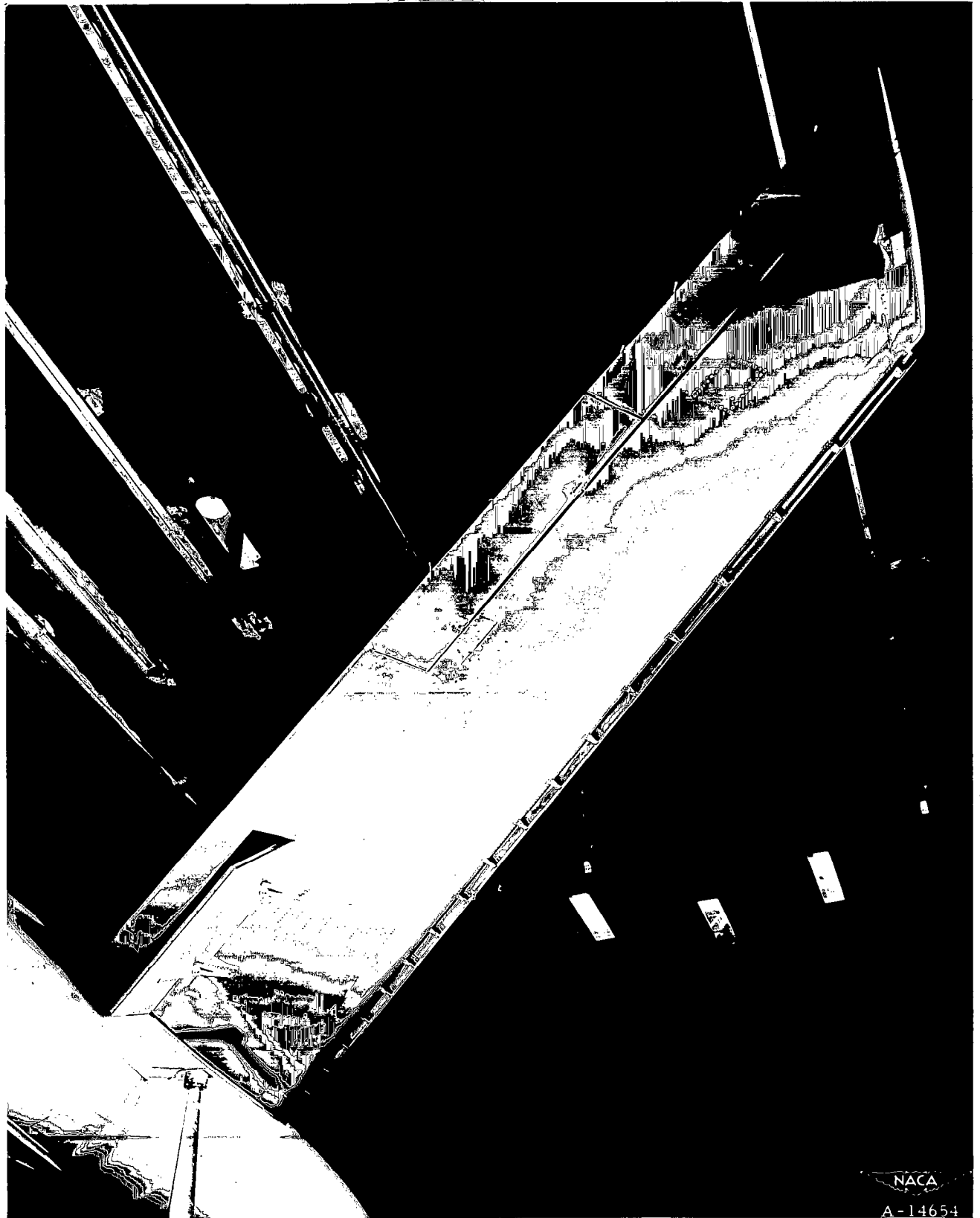
(a) General view with single fences.

Figure 7.- Photographs of the configurations tested.



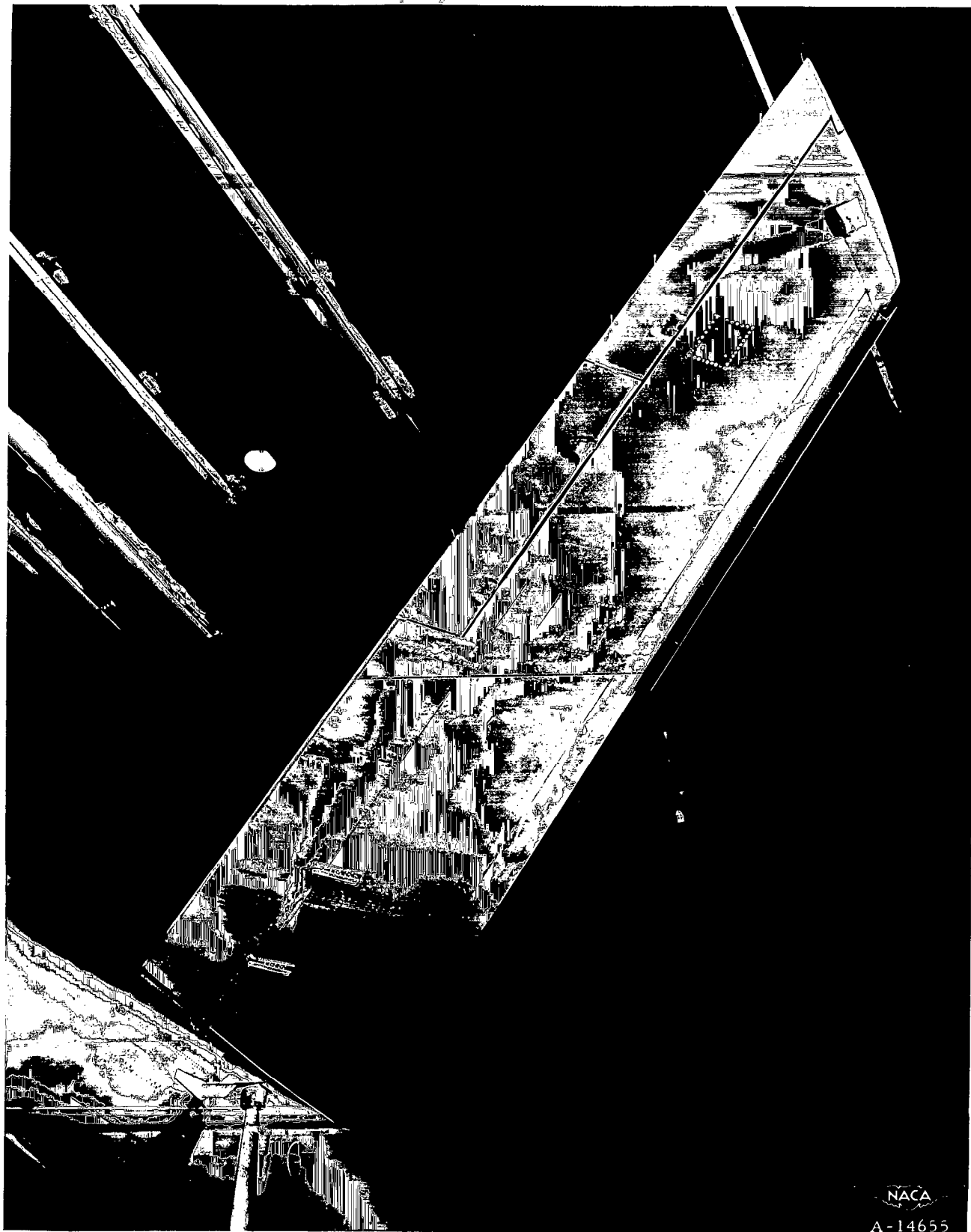
(b) Close-up of single fence.

Figure 7.- Continued.



(d) Close-up of lower surface of right wing with full-span leading-edge flap and trailing-edge flap deflected  $45^\circ$ .

Figure 7.- Continued.



(e) Close-up of lower surface of right wing with 30-percent-span leading-edge flap.

Figure 7.- Continued.

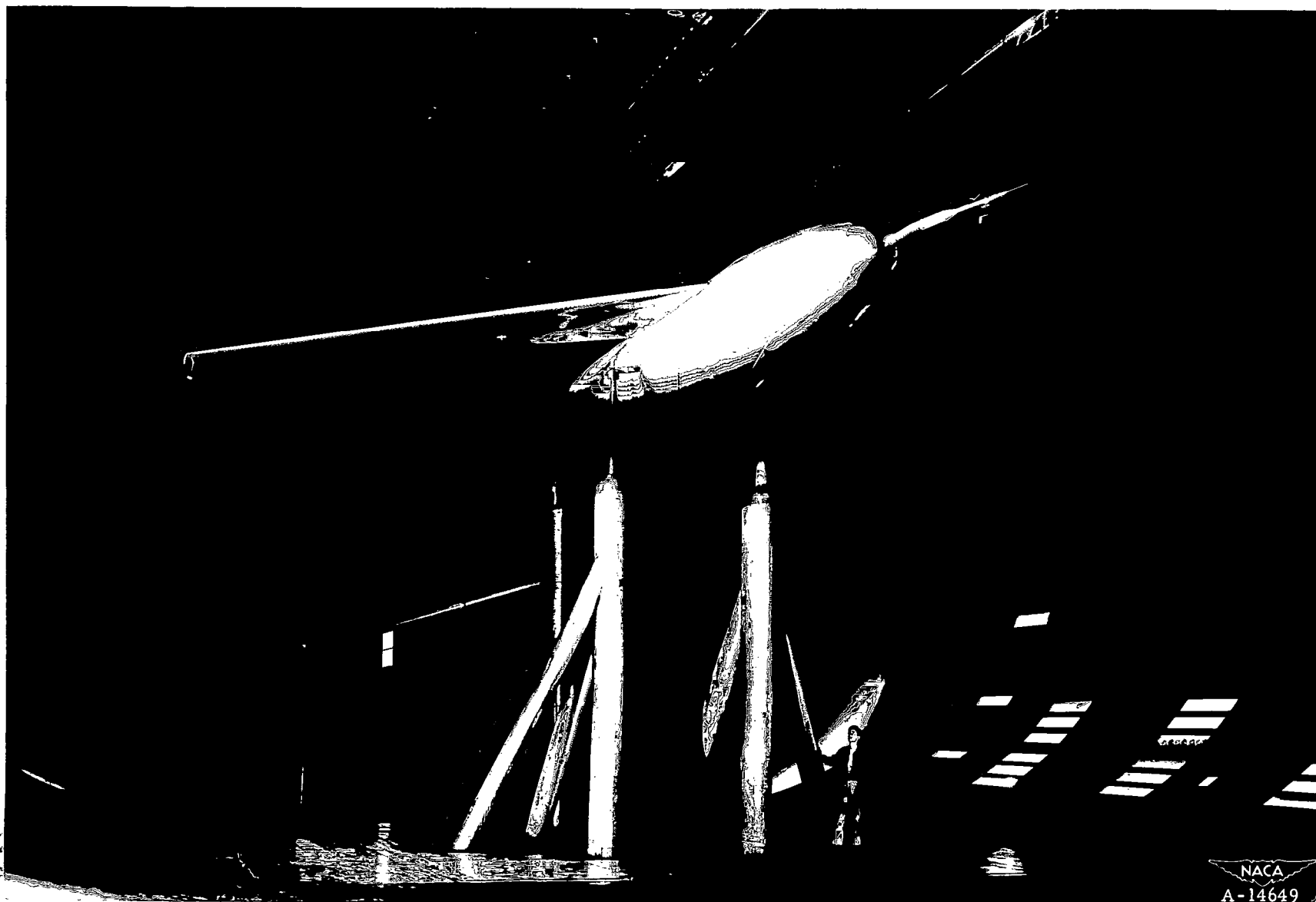


NACA

A-14656

(f) Close-up of lower surface of right wing with increased leading-edge radius.

Figure 7.- Continued.



(g) General view of model with increased leading-edge radius.

Figure 7.-- Concluded.

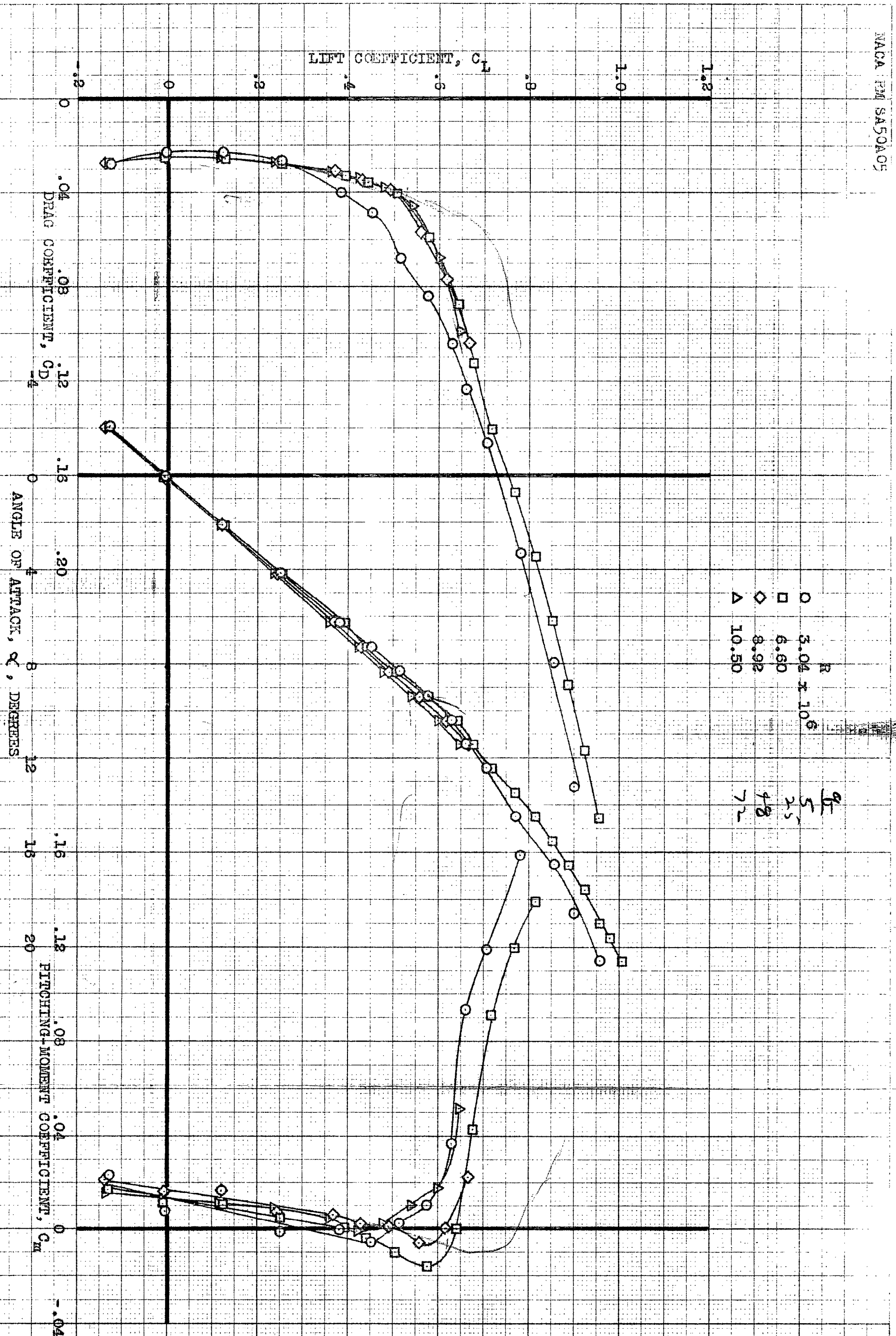


FIGURE 8. - AERODYNAMIC CHARACTERISTICS OF THE BASIC MODEL, WITHOUT TRAILING-EDGE FLAPS; VARIOUS REYNOLDS NUMBERS.

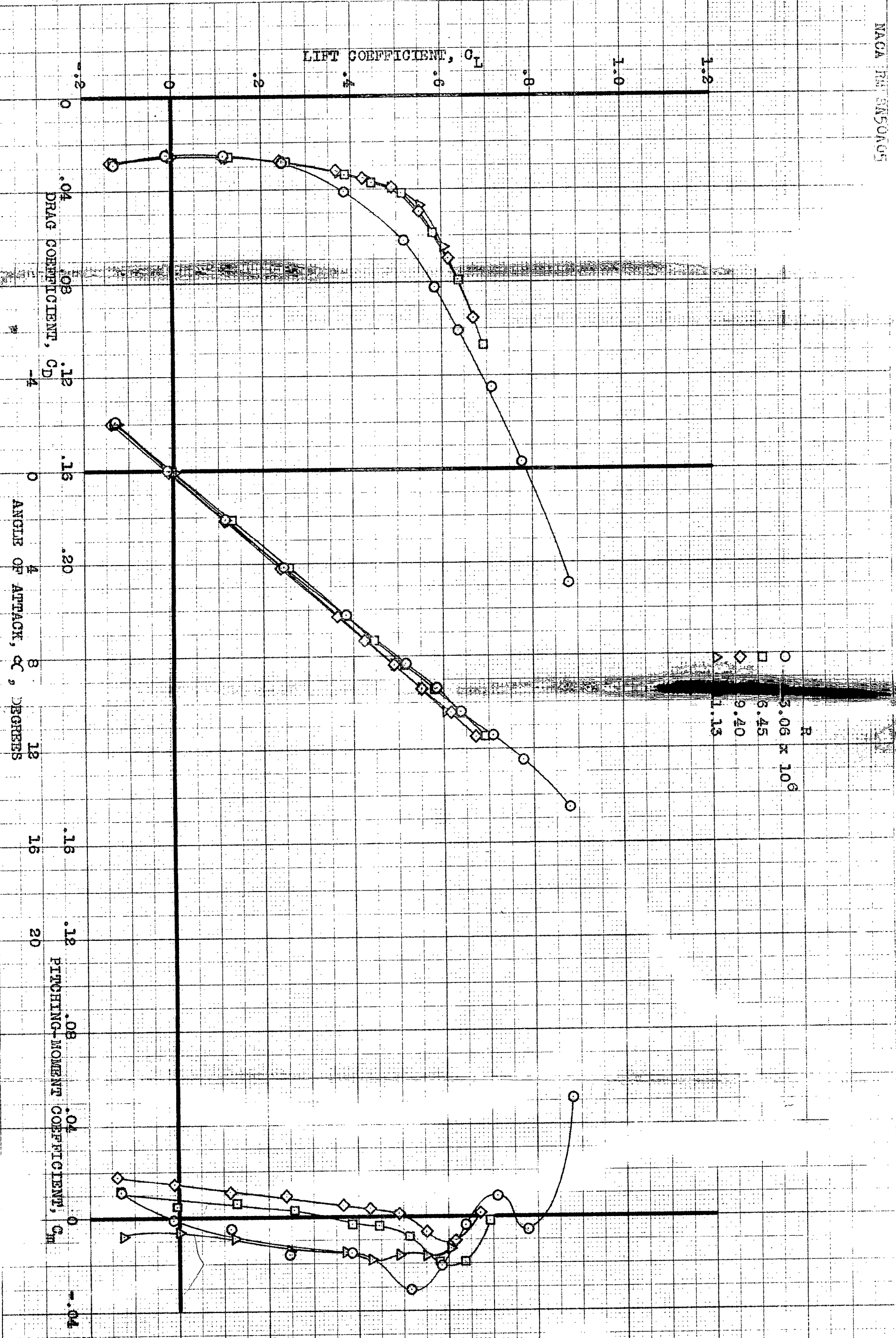
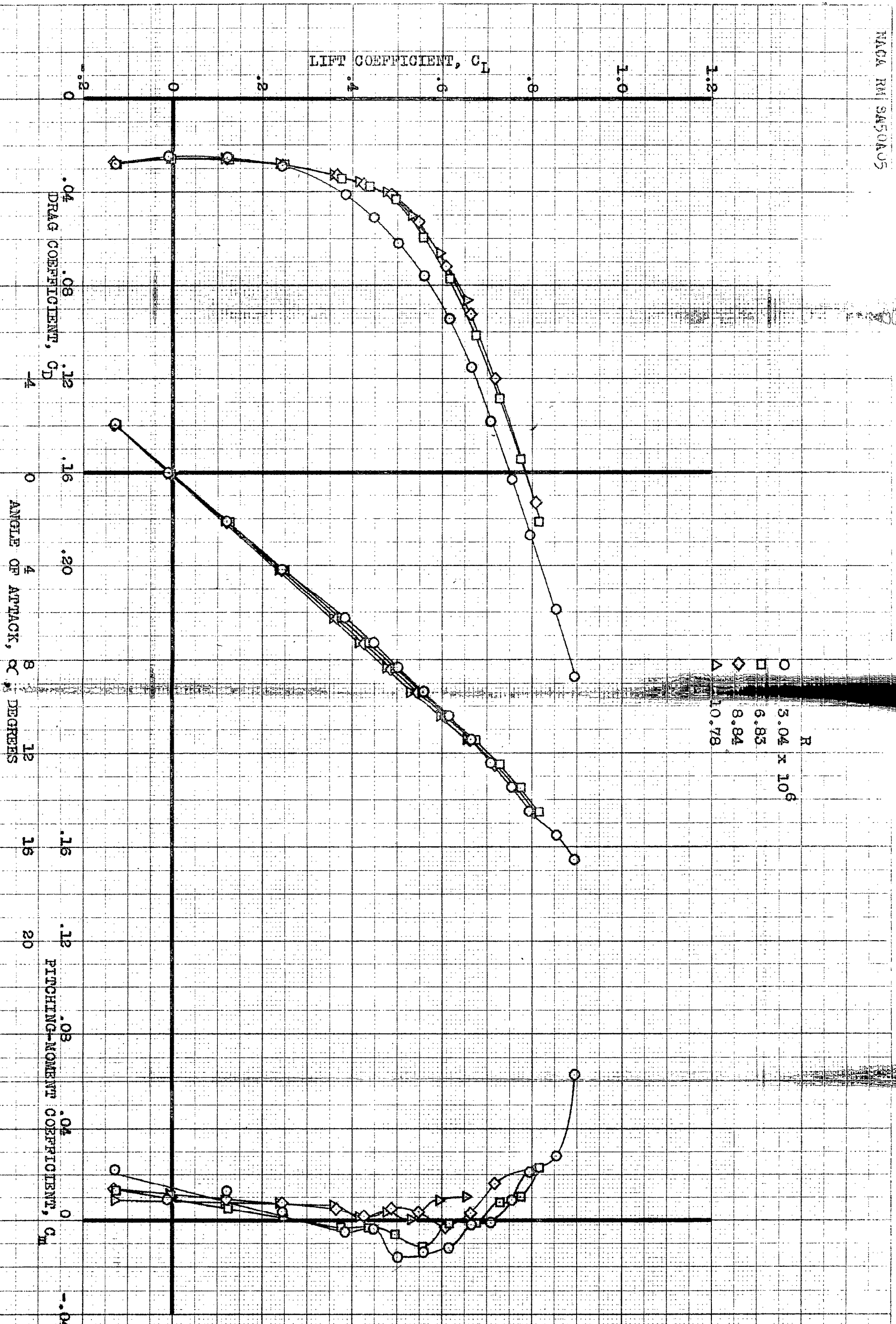
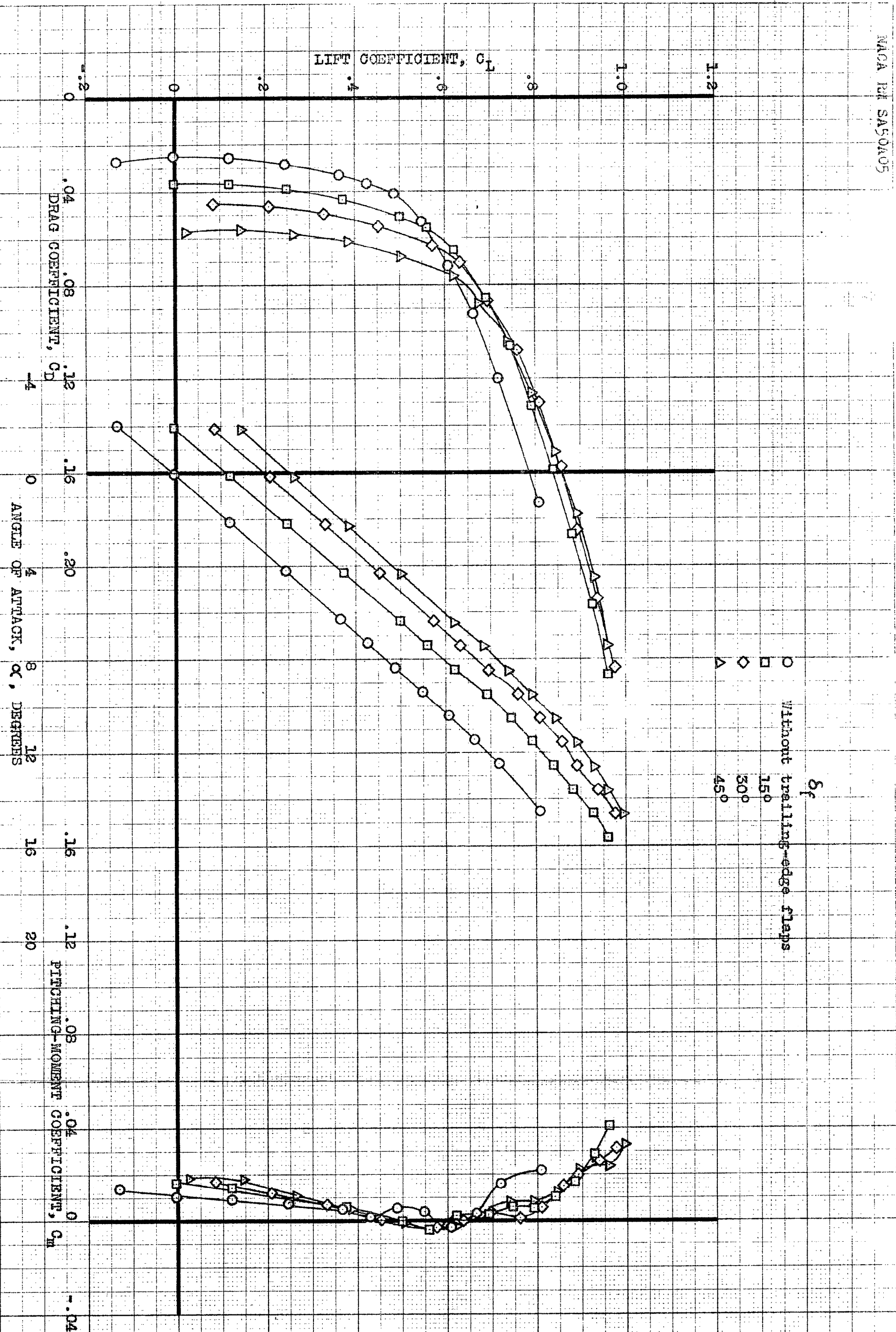


FIGURE 9. AERODYNAMIC CHARACTERISTICS OF THE MODEL WITH SINGLE FENCES, WITHOUT TRAILING-EDGE FLAPS; VARIOUS REYNOLDS NUMBERS.



(a) WITHOUT TRAILING-EDGE FLAPS; VARIOUS REYNOLDS NUMBERS.

FIGURE 10.- AERODYNAMIC CHARACTERISTICS OF THE MODEL WITH DOUBLE FENCES.



(b) TRAILING-EDGE FLAPS;  $R_e = 9 \times 10^6$ .

FIGURE 10. CONCLUDED.

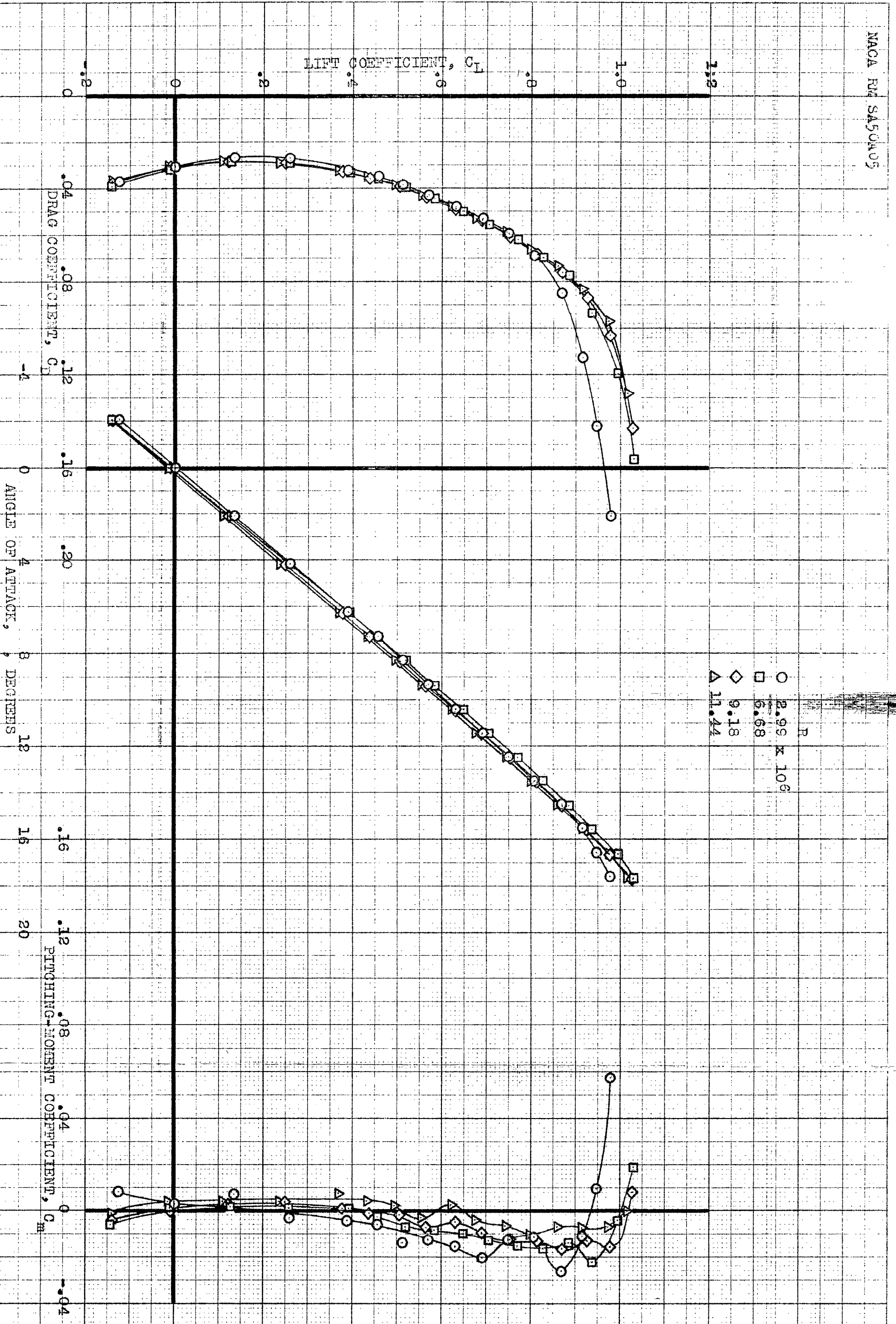


FIGURE 11.- AERODYNAMIC CHARACTERISTICS OF THE MODEL WITH FULL-SPAN LEADING-EDGE FLAPS; VARIOUS REYNOLDS NUMBERS.

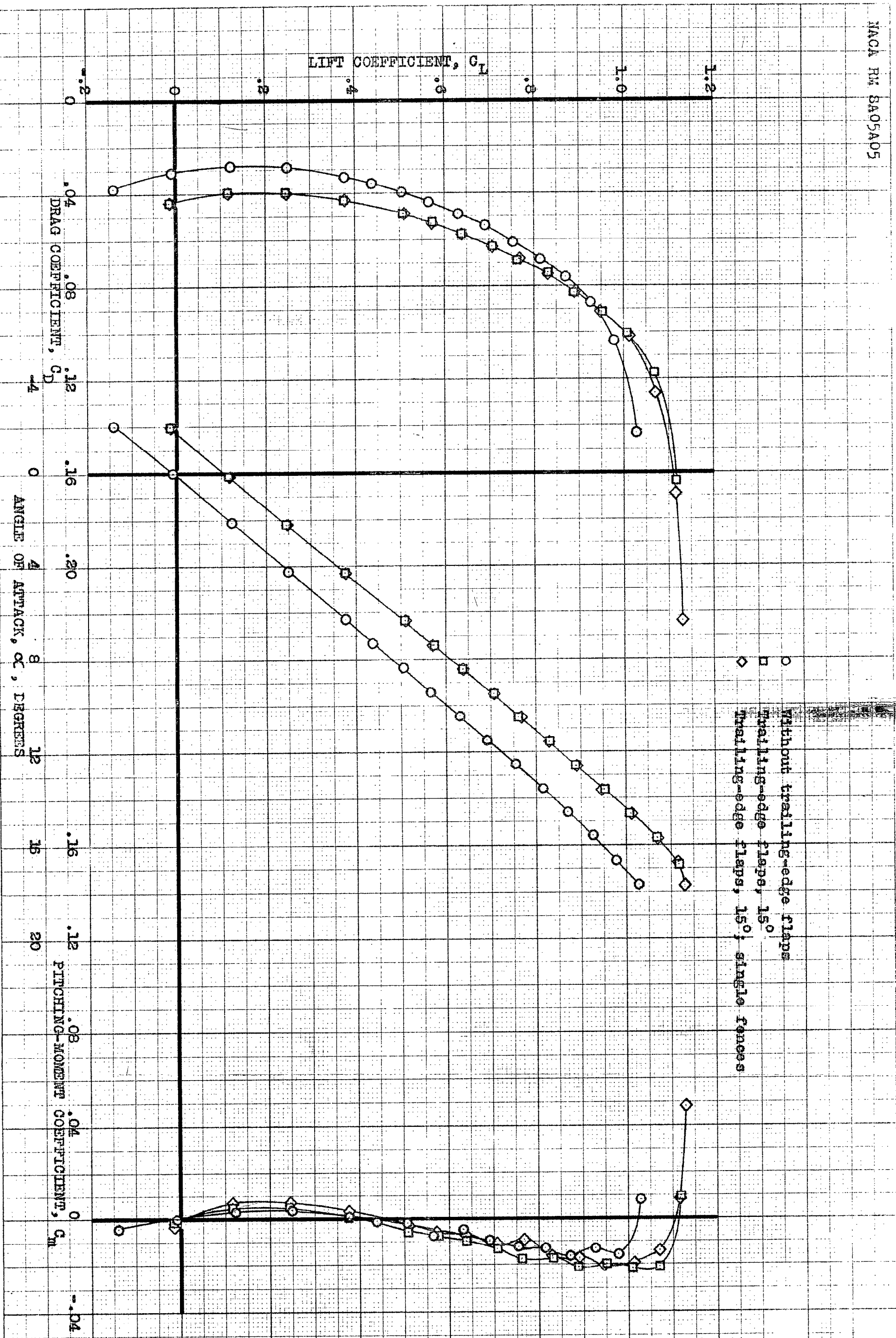
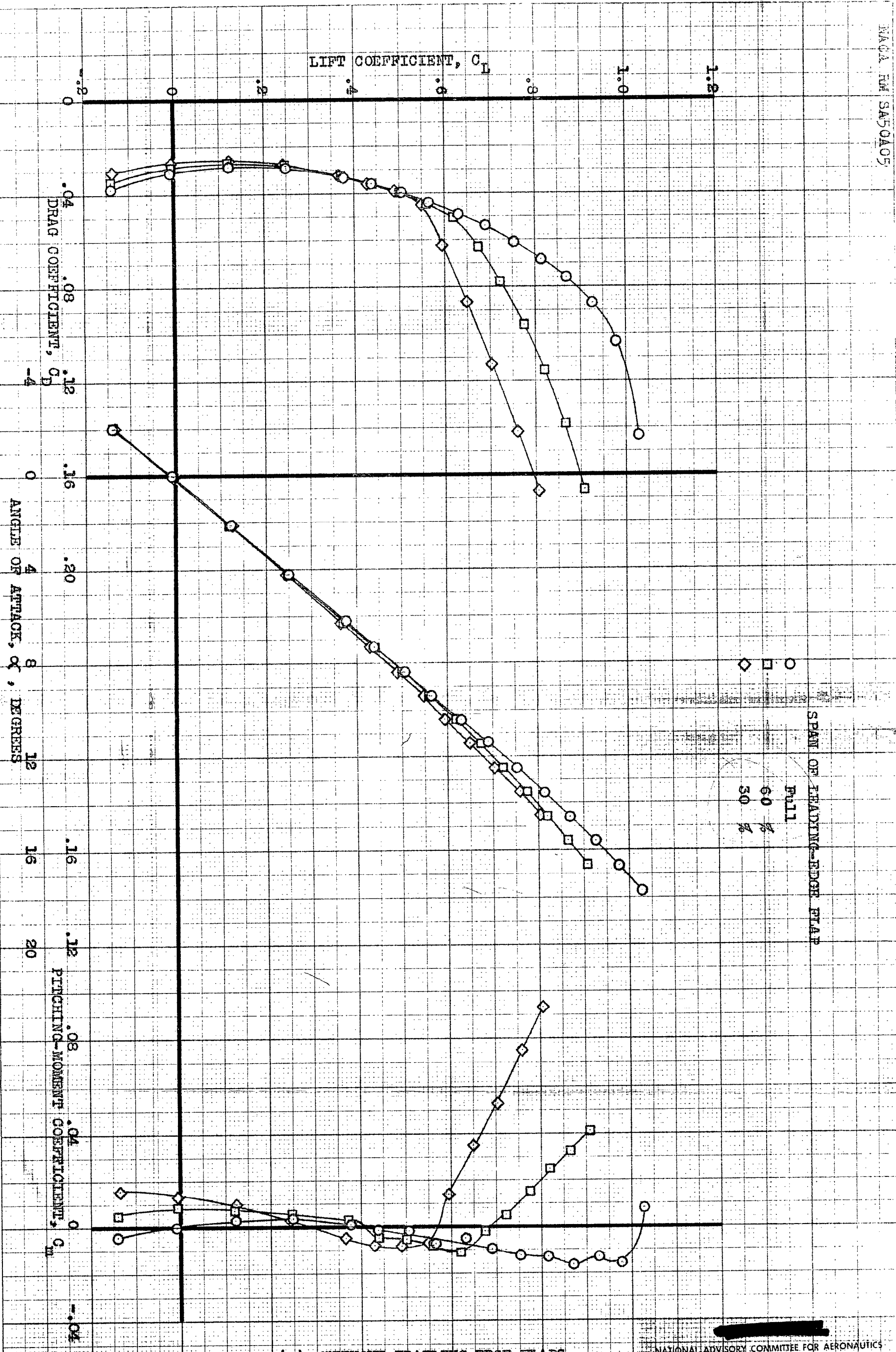


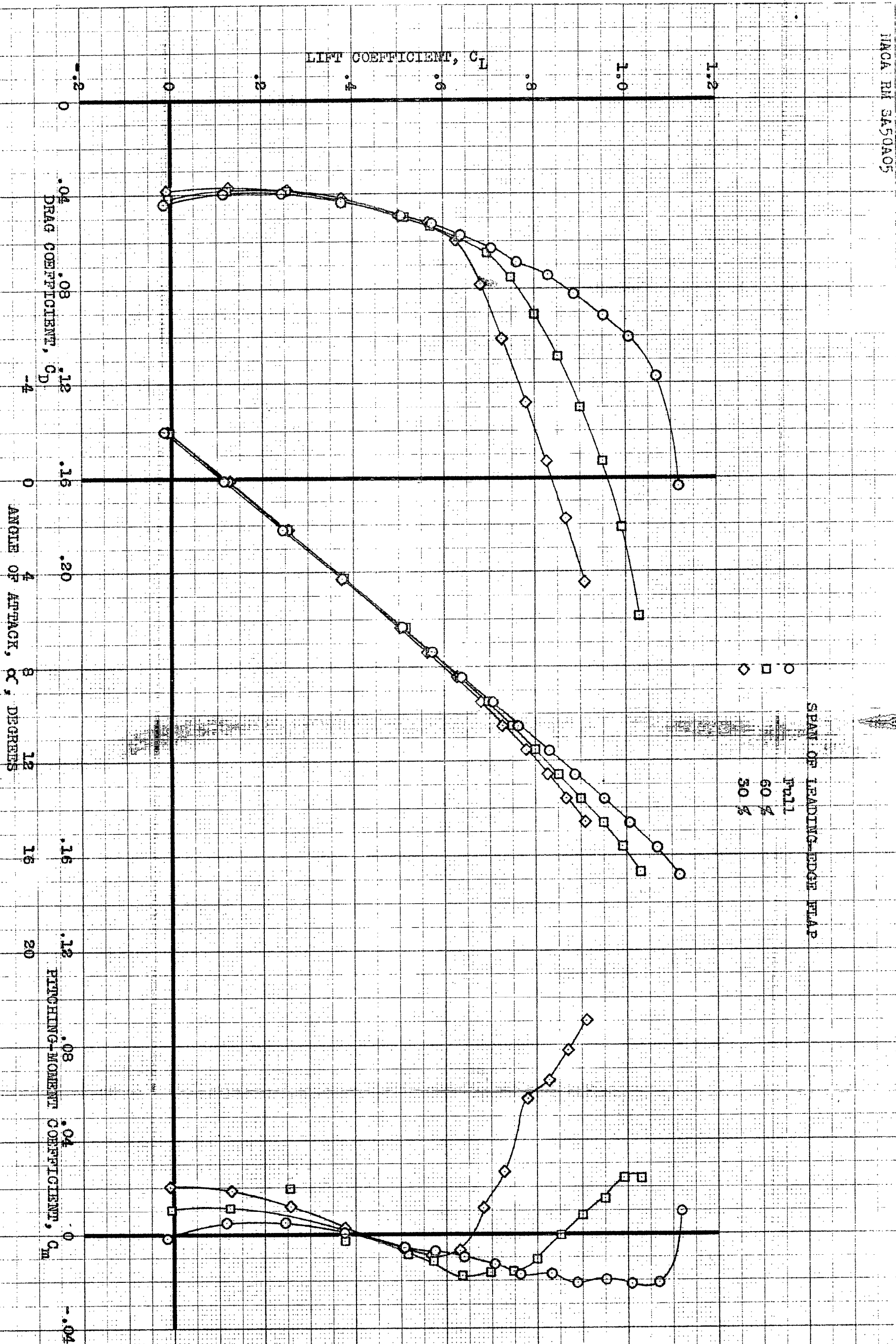
FIGURE 12.- AERODYNAMIC CHARACTERISTICS OF THE MODEL WITH FULL-SPAN LEADING-EDGE FLAPS IN COMBINATION WITH TRAILING-EDGE FLAPS AND SINGLE FENCES,  $R, 9 \times 10^6$ .



(a) WITHOUT TRAILING-EDGE FLAPS.

NATIONAL ADVISORY COMMITTEE FOR AERONAUTICS

FIGURE 13.- AERODYNAMIC CHARACTERISTICS OF THE MODEL WITH VARIOUS SPANS OF LEADING-EDGE FLAPS.  $R, 9 \times 10^6$ .



(b) TRAILING-EDGE FLAPS, 15°.

FIGURE 13.- CONCLUDED.

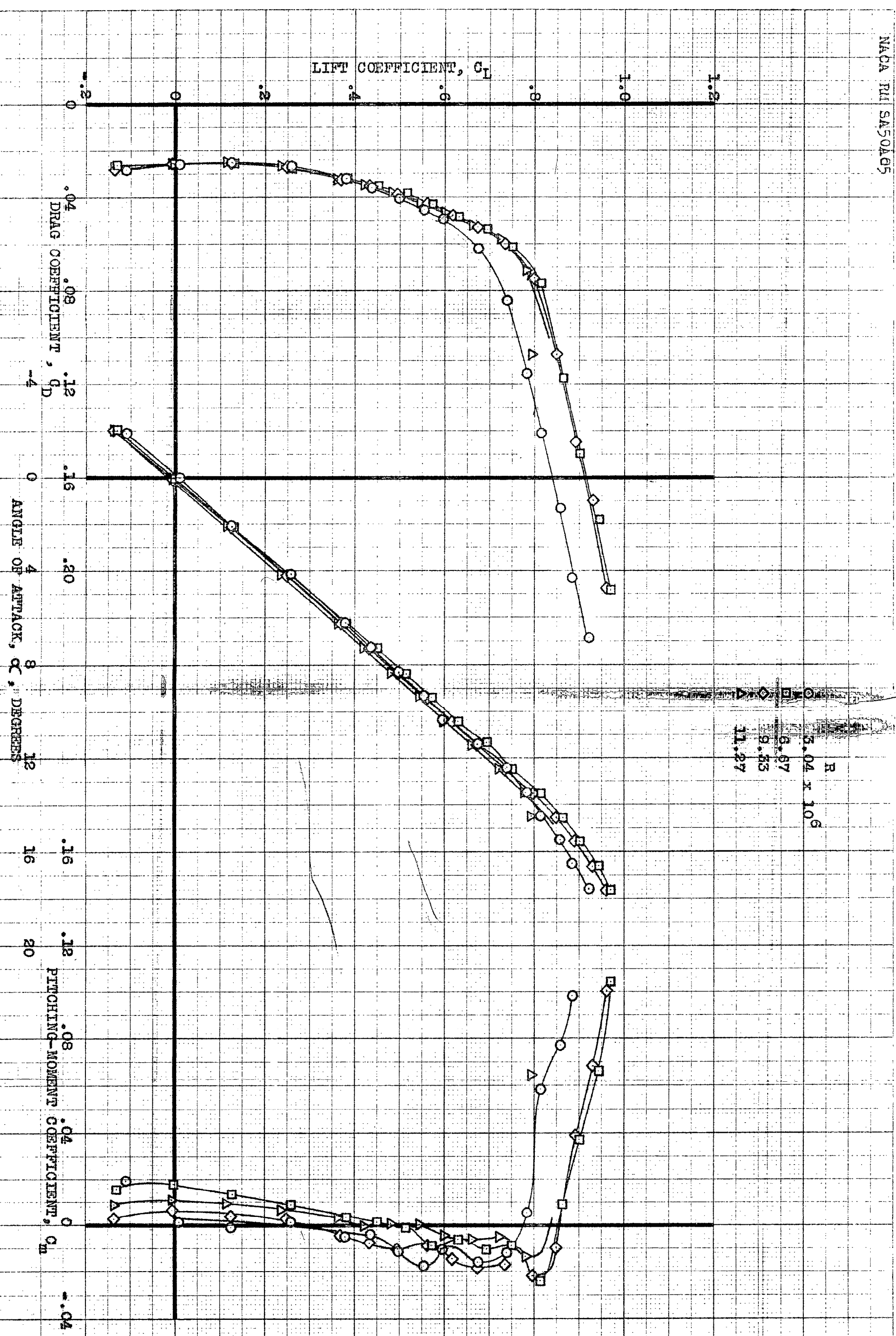
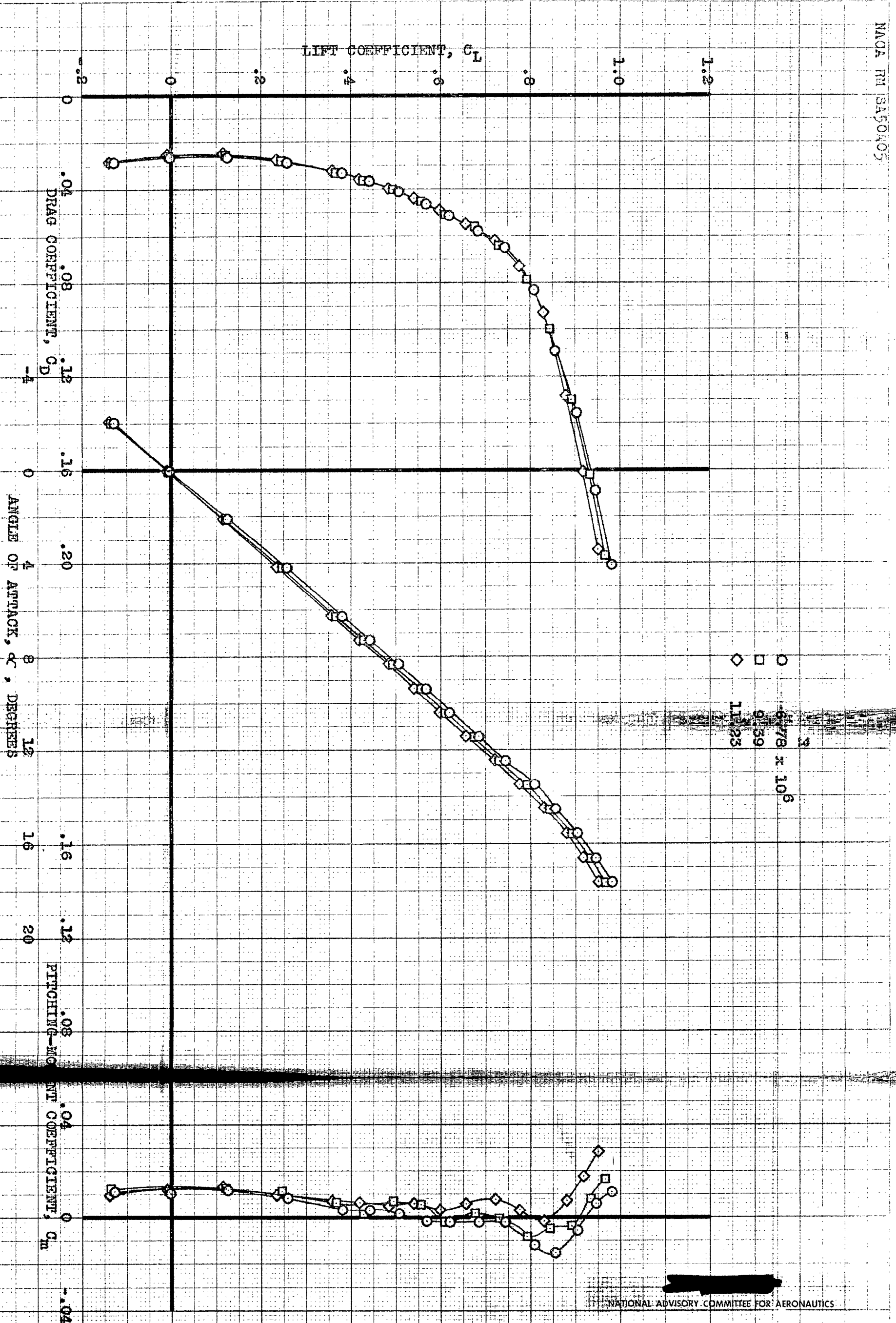


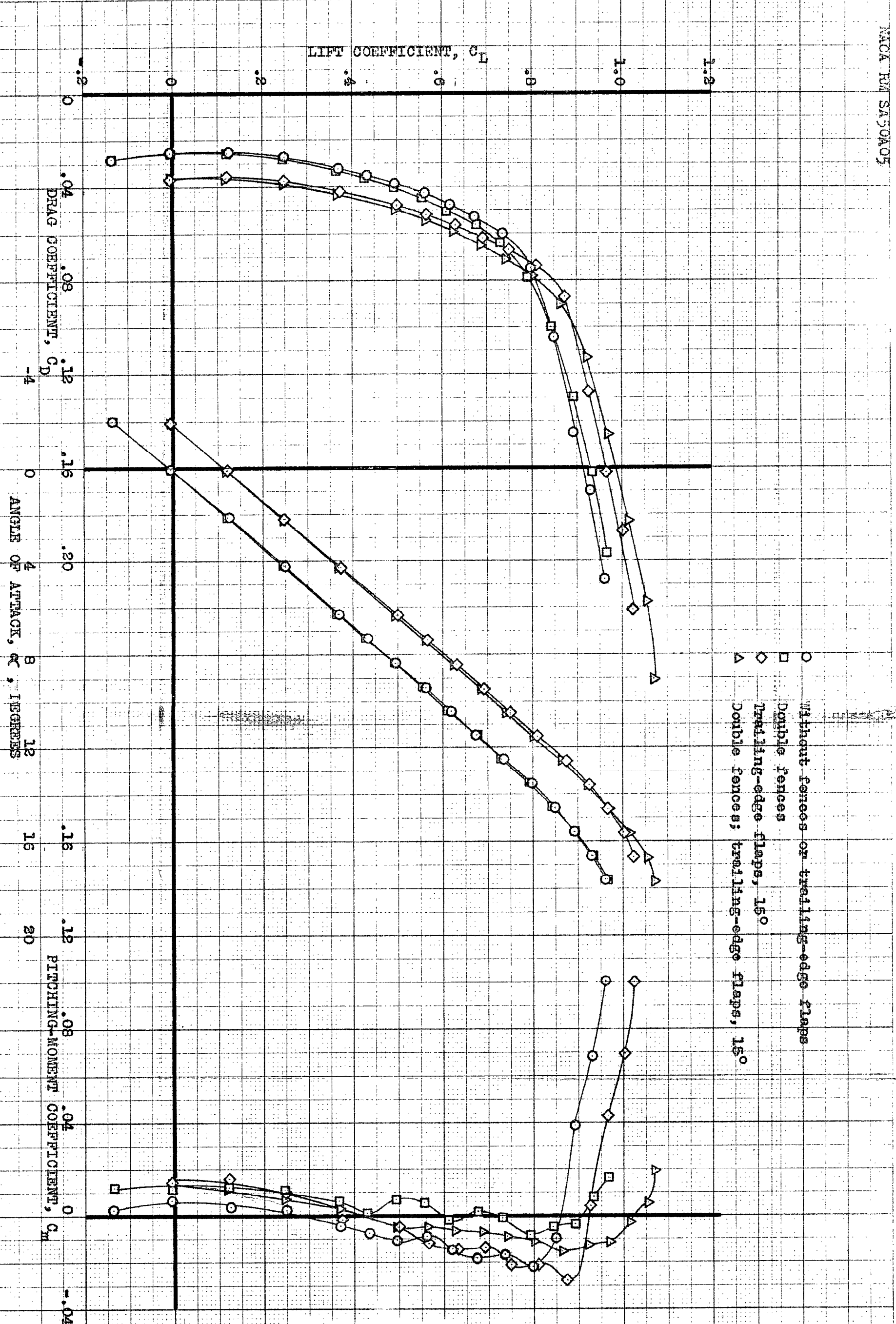
FIGURE 14.- AERODYNAMIC CHARACTERISTICS OF THE MODEL WITH INCREASED LEADING-EDGE RADIUS. VARIOUS REYNOLDS NUMBERS.



NATIONAL ADVISORY COMMITTEE FOR AERONAUTICS

(a) WITHOUT TRAILING-EDGE FLAPS; VARIOUS REYNOLDS NUMBERS; DOUBLE FENCES.

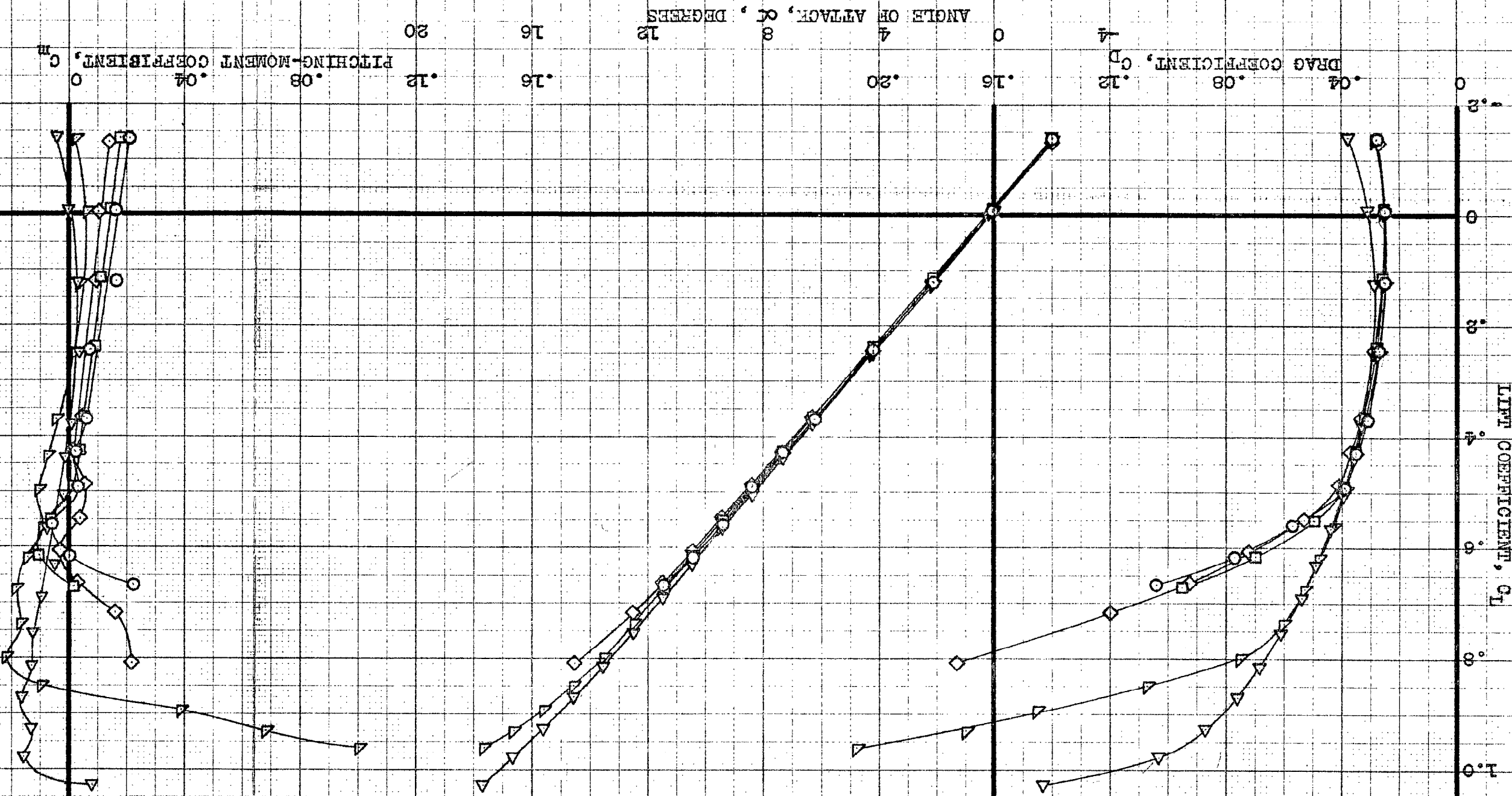
FIGURE 15.- AERODYNAMIC CHARACTERISTICS OF THE MODEL WITH INCREASED LEADING-EDGE RADIUS.



○ Without fences or trailing-edge flaps  
 □ Double fences  
 ◇ Trailing-edge flaps, 15°  
 △ Double fences; trailing-edge flaps, 15°

(b) VARIOUS CONFIGURATIONS;  $R, 9 \times 10^6$ .

FIGURE 15. CONCLUDED.

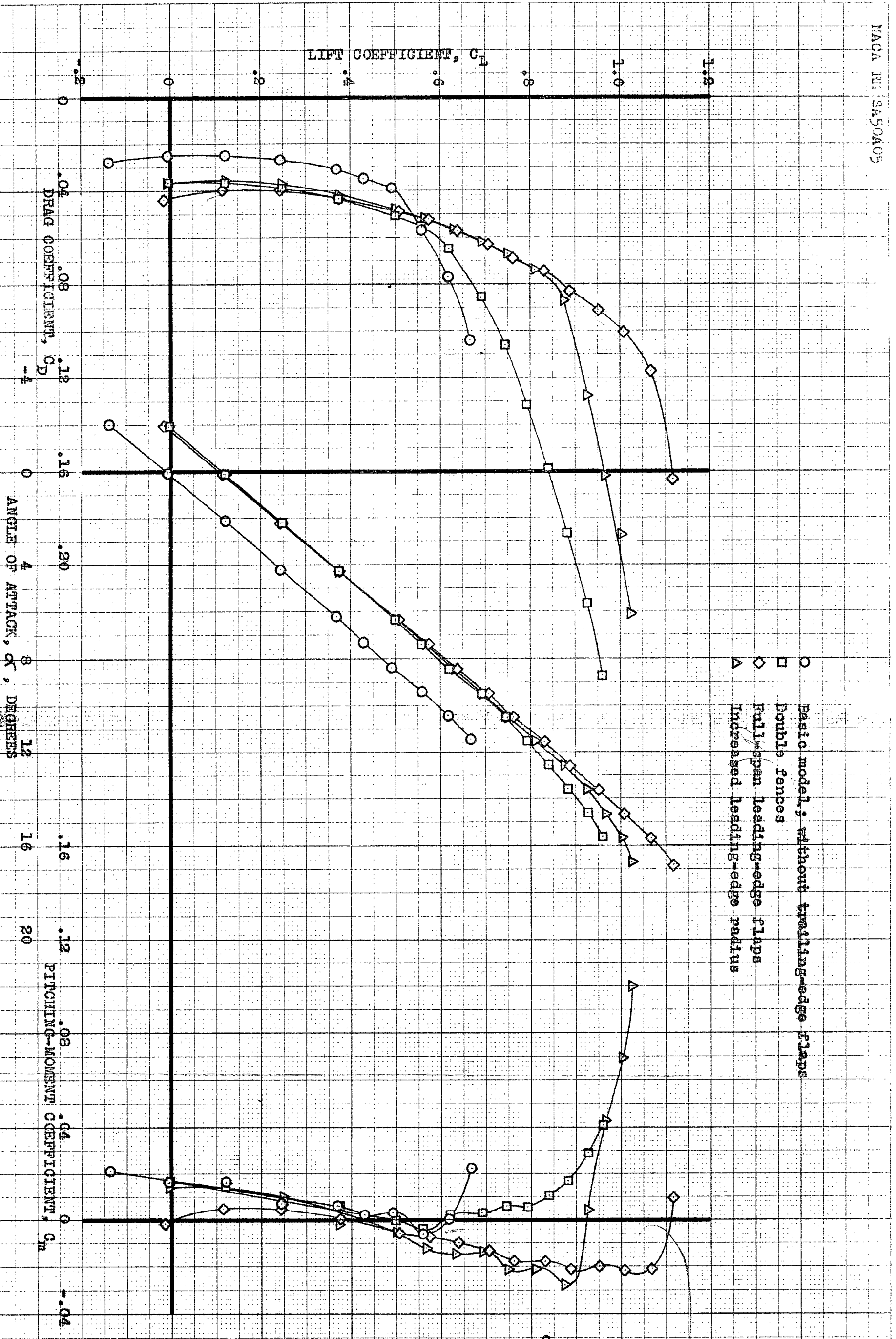


O Basile Model  
 □ Single fences  
 ◇ Double fences  
 ▽ Full-span leading-edge flaps  
 ▲ Increased leading-edge radius

(a) WITHOUT TRAILING-EDGE FLAPS.

FIGURE 16. COMPARISON OF THE AERODYNAMIC CHARACTERISTICS OF VARIOUS CONFIGURATIONS TESTED. R, 9 x 10<sup>5</sup>.

NATIONAL ADVISORY COMMITTEE FOR AERONAUTICS



(b) TRAILING-EDGE FLAPS, 15°.

FIGURE 16.- CONCLUDED.

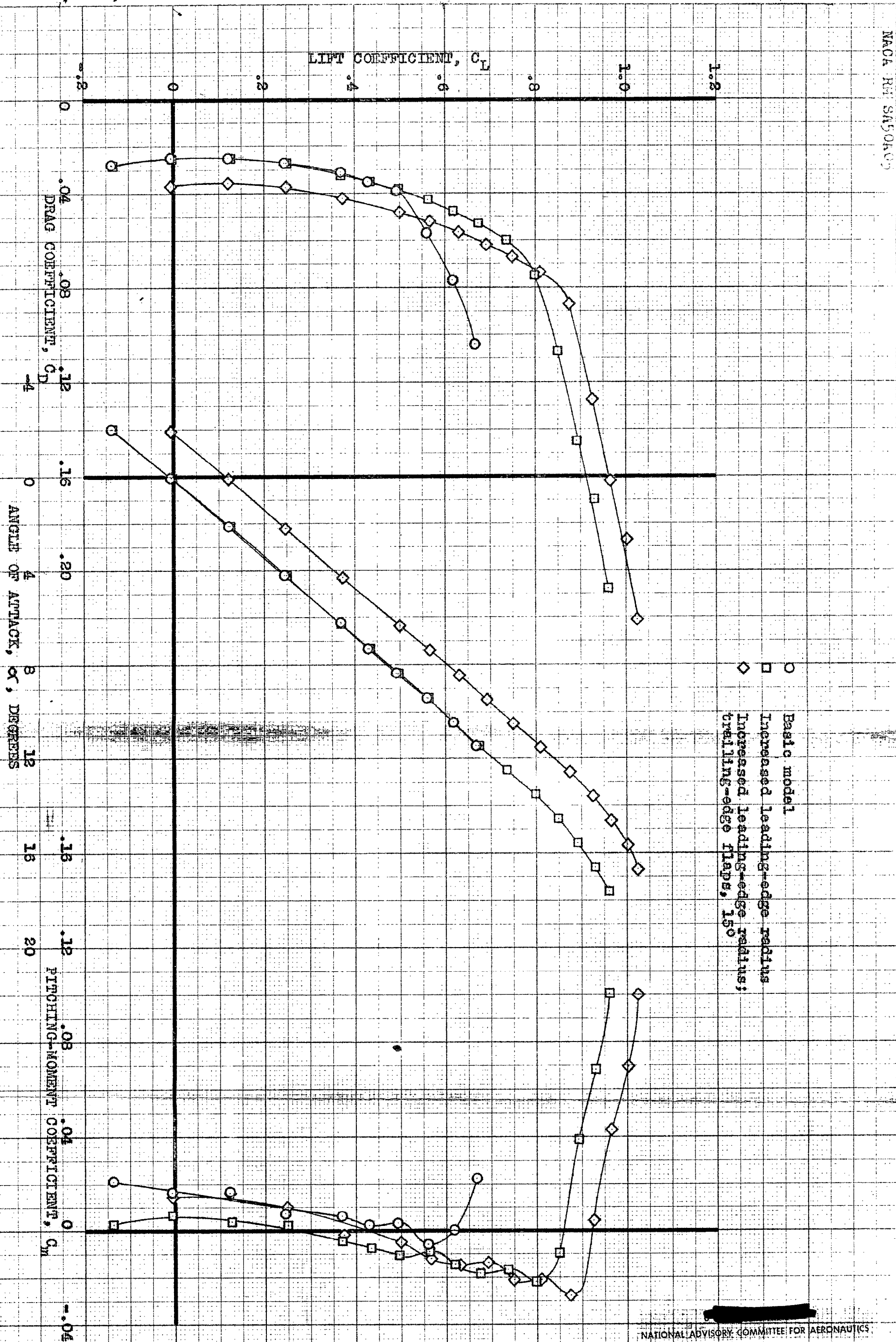


FIGURE 17.- COMPARISON OF THE AERODYNAMIC CHARACTERISTICS OF THE BASIC MODEL WITH THE CHARACTERISTICS OF THE MODEL WITH INCREASED LEADING-EDGE RADIUS, WITH AND WITHOUT TRAILING-EDGE FLAPS.  $R, 9 \times 10^6$ .

NASA Technical Library



3 1176 01437 2867